

1 **Spectral- and size-resolved mass absorption efficiency of mineral dust aerosols in**  
2 **the shortwave spectrum: a simulation chamber study**

3 Lorenzo Caponi<sup>1,2</sup>, Paola Formenti<sup>1</sup>, Dario Massabó<sup>2</sup>, Claudia Di Biagio<sup>1</sup>, Mathieu Cazaunau<sup>1</sup>, Edou-  
4 ard Pangui<sup>1</sup>, Servanne Chevaillier<sup>1</sup>, Gautier Landrot<sup>3</sup>, Meinrat O. Andreae<sup>4,11</sup>, Konrad Kandler<sup>5</sup>, Stuart  
5 Piketh<sup>6</sup>, Thuraya Saeed<sup>7</sup>, Dave Seibert<sup>8</sup>, Earle Williams<sup>9</sup>, Yves Balkanski<sup>10</sup>, Paolo Prati<sup>2</sup>, and Jean-  
6 François Doussin<sup>1</sup>

7 <sup>1</sup> *Laboratoire Interuniversitaire des Systèmes Atmosphériques (LISA), UMR 7583, CNRS, Université Paris-Est-*  
8 *Créteil et Université Paris Diderot, Institut Pierre Simon Laplace, Créteil, France*

9 <sup>2</sup> *University of Genoa, Department of Physics & INFN, Genoa, Italy*

10 <sup>3</sup> *Synchrotron SOLEIL, L'Orme des Merisiers Saint-Aubin, France*

11 <sup>4</sup> *Biogeochemistry Department, Max Planck Institute for Chemistry, P.O. Box 3060, 55020, Mainz, Germany*

12 <sup>5</sup> *Institut für Angewandte Geowissenschaften, Technische Universität Darmstadt, Schnittspahnstr. 9, 64287*  
13 *Darmstadt, Germany*

14 <sup>6</sup> *Climatology Research Group, University of the Witwatersrand, Johannesburg, South Africa*

15 <sup>7</sup> *Science Department, College of Basic Education, Public Authority for Applied Education and Training, Al-*  
16 *Ardeya, Kuwait*

17 <sup>8</sup> *Walden University, Minneapolis, Minnesota, USA*

18 <sup>9</sup> *Massachusetts Institute of Technology, Cambridge, Massachusetts, USA*

19 <sup>10</sup> *LSCE, CNRS UMR 8212, CEA, Université de Versailles Saint-Quentin, Gif sur Yvette, France*

20 <sup>11</sup> *Geology and Geophysics Department, King Saud University, Riyadh, Saudi Arabia*

21  
22 \* Corresponding author: [paola.formenti@lisa.u-pec.fr](mailto:paola.formenti@lisa.u-pec.fr)  
23

## 24 Abstract

25 This paper presents new laboratory measurements of the mass absorption efficiency (MAE) between  
26 375 and 850 nm for [twelve individual samples of](#) mineral dust [from different source areas worldwide](#)  
27 [and in of different origin](#) in two size classes: PM<sub>10.6</sub> (mass fraction of particles of aerodynamic diameter  
28 lower than 10.6 μm) and PM<sub>2.5</sub> (mass fraction of particles of aerodynamic diameter lower than 2.5 μm).  
29 ~~The~~ experiments ~~have been~~ were performed in the CESAM simulation chamber using ~~generated~~-min-  
30 eral dust generated from natural parent soils, and included optical and gravimetric analyses.

31 ~~The R~~results show that the MAE values are lower for the PM<sub>10.6</sub> mass fraction (range 37-135 10<sup>-3</sup> m<sup>2</sup> g<sup>-1</sup>  
32 at 375 nm) than for the PM<sub>2.5</sub> (range 95-711 10<sup>-3</sup> m<sup>2</sup> g<sup>-1</sup> at 375 nm), and decrease with increasing wave-  
33 length as  $\lambda^{-AAE}$ , where the Angstrom Absorption Exponent (AAE) averages between 3.3-3.5, regardless  
34 of size. The size-independence of AAE suggests that, for a given size distribution, the ~~possible variation~~  
35 ~~of dust composition~~ did not vary with size for this set of samples~~with size would not affect significantly~~  
36 ~~the spectral behavior of shortwave absorption~~. Because of its high atmospheric concentration, light-  
37 absorption by mineral dust can be competitive ~~to~~ with black and brown carbon even during atmospheric  
38 transport over heavy polluted regions, when dust concentrations are significantly lower than at emission.  
39 The AAE values of mineral dust are higher than for black carbon (~1), but in the same range as light-  
40 absorbing organic (brown) carbon. As a result, depending on the environment, there can be some ambi-  
41 guity in apportioning the aerosol absorption optical depth (AAOD) based on spectral dependence, which  
42 is relevant to the development of remote sensing of light-absorbing aerosols ~~from space~~, and their  
43 assimilation in climate models. We suggest that the sample-to-sample variability in our dataset of MAE  
44 values is related to regional differences ~~of in~~ the mineralogical composition of the parent soils. Particu-  
45 larly in the PM<sub>2.5</sub> fraction, we found a strong linear correlation between the dust light-absorption prop-  
46 erties and elemental iron rather than the iron oxide fraction, which could ease the application and the  
47 validation of climate models that now start to include the representation of the dust composition, as well  
48 as for remote sensing of dust absorption in the UV-VIS spectral region.

## 49 1. Introduction

50 Mineral dust aerosols emitted by wind erosion of arid and semi-arid soils account for about 40% of the  
51 total emitted aerosol mass per year at the global scale (Knippertz and Stuut, 2014). The episodic but  
52 frequent transport of intense mineral dust plumes is visible from spaceborne sensors, as their high con-  
53 centrations, combined with ~~to~~ their ability of to scattering and absorbing solar and thermal radiation,

54 give raise to the highest registered values of aerosol optical depth (AOD) on Earth (Chiapello, 2014).  
55 The instantaneous radiative efficiency of dust particles, that is, their radiative effect per unit AOD, is of  
56 the order of tenths to hundreds of  $W m^{-2} AOD^{-1}$  in the solar spectrum, and of the order of order of tenths  
57 of  $W m^{-2} AOD^{-1}$  in the thermal infrared (e.g., Haywood et al., 2003; di Sarra et al., 2011; Slingo et al.,  
58 2006 and the compilation of Highwood and Ryder, 2014). ~~In the solar spectrum, (Boucher et al., 2013).~~  
59 Albeit partially compensated by the radiative effect in the thermal infrared, the global mean radiative  
60 effect of mineral dust in the shortwave is negative both at the surface and the top of the atmosphere  
61 (TOA) and produces a local warming of the atmosphere (Boucher et al., 2013). ~~Many-There are the~~  
62 ~~consequences- numerous impacts of dust on the~~ global and regional climate, ~~that-which~~ ultimately feed  
63 back on wind speed and vegetation and therefore on dust emission (Tegen and Lacis, 1996; Solmon et  
64 al., 2008; Pérez et al., 2006; Miller et al., 2014). Dust particles perturb the surface air temperature  
65 through their radiative effect at TOA, can increase the atmospheric stability (e.g., Zhao et al. 2011) and  
66 might affect precipitation at the global and regional scale (Solmon et al., 2008; Xian, 2008; Vinoj et al.,  
67 2014; Miller et al., 2014 and references therein).

68 All models ~~show- indicate~~ that the effect of mineral dust on climate has a great sensitivity to their  
69 shortwave absorption properties ~~of mineral dust~~ (Miller et al., 2004; Lau et al., 2009; Loeb and Su, 2010;  
70 Ming et al., 2010; Perlwitz and Miller, 2010). Absorption by mineral dust started receiving a great deal  
71 of interest ~~in the last ten years or so~~, when spaceborne and ground-based remote sensing studies (Dubovik  
72 et al., 2002; Colarco et al., 2002; Sinyuk et al., 2003) suggested that mineral dust was less absorbing  
73 ~~that- than it~~ had been ~~suggested indicated~~ by in situ observations (e.g., Patterson et al., 1977; Haywood et  
74 al., 2001), particularly at wavelengths below 600 nm. Balkanski et al. (2007) showed that lowering the  
75 dust absorption properties to an extent that reconciles them both with the remote-sensing observations  
76 and the state-of-knowledge of the mineralogical composition, allowed calculating the clear-sky dust  
77 shortwave radiative effect of dust in agreement with satellite-based observations. A significant body  
78 number of observations has ~~ve been performed in quantify~~ quantified the shortwave light-absorbing  
79 properties of mineral dust, by direct measurements (Alfaro et al., 2004; Linke et al., 2006; Osborne et  
80 al., 2008; McConnell et al., 2008; Derimian et al., 2008; Yang et al., 2009; Müller et al., 2009; Petzold  
81 et al., 2009; Formenti et al., 2011; Moosmüller et al., 2012; Wagner et al., 2012; Ryder al., 2013a; Utry  
82 et al., 2015; Denjean et al., 2015c; 2016), and indirectly, by quantifying the amount and the speciation  
83 of the light-absorbing compounds in mineral dust, principally iron oxides (Lafon et al., 2004; 2006;

84 Lazaro et al., 2008; Derimian et al., 2008; Zhang et al., 2008; Kandler et al., 2007; 2009; 2011; Formenti  
85 et al., 2014a; 2014b).

86 However, existing data are often limited to a single wavelength, which moreover ~~are-is~~ not the same  
87 identical for all experiments. Also, frequently they do not represent the possible regional variability of  
88 the dust absorption, either because they are obtained from field measurements integrating the contribu-  
89 tions of different source regions, or conversely, by laboratory investigations targeting samples from a  
90 limited number of locations. This might lead to biases in the data. Indeed, iron oxides in mineral dust,  
91 mostly in the form of hematite ( $\text{Fe}_2\text{O}_3$ ) and goethite ( $\text{Fe}(\text{O})\text{OH}$ ), have specific absorption bands in the  
92 UV-VIS spectrum (Bédidi and Cervelle, 1993), and have a variable content depending on the soil min-  
93 eralogy of the source regions (Journet et al., 2014).

94 ~~Henceforth, in this study, experiments on twelve aerosol samples generated from natural parent top~~  
95 ~~soils from various source regions worldwide have been~~ conducted with a large atmospheric simu-  
96 lation chamber. ~~we~~ We present a new evaluation of the ultraviolet to near-infrared (375-850 nm) light-  
97 absorbing properties of mineral dust by studying-investigating the size-segregated mass absorption effi-  
98 ciency (MAE, units of  $\text{m}^2 \text{g}^{-1}$ ) and its spectral dependence, largely-widely used in climate models to  
99 calculate the direct radiative effect of aerosols. ~~Experiments on twelve aerosol samples generated from~~  
100 ~~natural parent top soils from various source regions worldwide have been conducted with a large atmos-~~  
101 ~~pheric simulation chamber.~~

## 102 2. Instruments and methods

103 At a given wavelength,  $\lambda$ , the mass absorption efficiency (MAE, units of  $\text{m}^2 \text{g}^{-1}$ ) is defined as the ratio  
104 of the aerosol light-absorption coefficient  $b_{\text{abs}}(\lambda)$  (units of  $\text{m}^{-1}$ ), and its mass concentration (in  $\mu\text{g m}^{-3}$ )

105

$$106 \quad MAE(\lambda) = \frac{b_{\text{abs}}(\lambda)}{\text{Mass Conc}} \quad (1)$$

107

108 ~~MAE values for mineral dust aerosol are expressed in~~ MAE values for mineral dust aerosol are ex-  
109 pressed in  $10^{-3} \text{m}^2 \text{g}^{-1}$ .

110 The spectral dependence of the aerosol absorption coefficient  $b_{\text{abs}}(\lambda)$  is described by the power-law  
111 relationship

112

113

$$b_{abs}(\lambda) \sim \lambda^{-AAE} \quad (2)$$

114

115 where the AAE is the [Absorption Ångström Absorption](#)-Exponent, representing the negative slope of  
116  $b_{abs}(\lambda)$  in a log-log plot (Moosmüller et al., 2009)

117

$$AAE = -\frac{d\ln(b_{abs}(\lambda))}{d\ln(\lambda)} \quad (3)$$

118

## 120 **2.1. The CESAM simulation chamber**

121 [The e](#)Experiments in this work have been performed in the 4.2 m<sup>3</sup> stainless-steel CESAM (French acro-  
122 nym for Experimental Multiphasic Atmospheric Simulation Chamber) simulation chamber (Wang et al.,  
123 2011). The CESAM chamber has been extensively used in recent years to simulate, at sub and super-  
124 saturated conditions, the formation and properties of aerosols at concentration levels comparable to those  
125 encountered in the atmosphere (Denjean et al., 2015a; 2015b; [Brégonzio-Rozier et al., 2015; 2016; Di](#)  
126 [Biagio et al., 2014; 2017](#)).

127 CESAM is a multi-instrumented platform, equipped with twelve circular flanges to support its analytical  
128 environment. Basic instrumentation comprises sensors to measure the temperature, pressure and relative  
129 humidity within the chamber (two manometers MKS Baratrons (MKS, 622A and MKS, 626A) and a  
130 HMP234 Vaisala® humidity and temperature sensor). The particle size distribution is routinely meas-  
131 ured by a combination of (i) a scanning mobility particle sizer (SMPS, mobility diameter range 0.02–  
132 0.88 µm), composed of a Differential Mobility Analyzer (DMA, TSI Inc. Model 3080) and a Condensa-  
133 tion Particle Counter (CPC, TSI Inc. Model 3772); (ii) a SkyGrimm optical particle counter (Grimm  
134 Inc., model 1.129, optical equivalent diameter range 0.25–32 µm); and (iii) a WELAS optical particle  
135 counter (PALAS, model 2000, optical equivalent diameter range 0.5–47 µm). Full details of operations  
136 and data treatment of the particle counters are provided in [Di Biagio et al. \(2016, 2017\)](#).

## 137 **2.2. Filter sampling**

138 Three filter samples per top soil sample were collected on different types of substrate based on the anal-  
139 ysis to [be performed](#). Sampling dedicated to the determination of the aerosol mass concentration by

140 gravimetric analysis and the measurement of the absorption coefficients by optical analysis was per-  
141 formed on 47-mm quartz membranes (Pall Tissuquartz™, 2500 QAT-UP). Two samples were collected  
142 in parallel. The first quartz membrane sample (“total”) was collected without a dedicated size cut-off  
143 using an in-house built stainless steel sampler operated at 5 L min<sup>-1</sup>. However, as detailed in Di Biagio  
144 et al. (2016, 2017), the length of the sampling line from the intake point in the chamber to the filter en-  
145 trance was 50 cm, yielding resulting in with a 50% cut-off of the transmission efficiency at 10.6 μm in  
146 particle aerodynamic diameter. This fraction is therefore indicated as PM<sub>10.6</sub> in the forthcoming follow-  
147 ing discussion. The second quartz membrane sample was collected using a 4-stage DEKATI impactor  
148 operated at the a flow rate of 10 L min<sup>-1</sup> to select the aerosol fraction of particles with aerodynamic  
149 diameter smaller than 2.5 μm, indicated as PM<sub>2.5</sub> here forth. Sampling for the analysis of the iron oxide  
150 content was performed on polycarbonate filters (47-mm Nuclepore, Whatman; pore size of 0.4 μm)  
151 using the same sample holder than as used for the total quartz filters, and therefore referring correspond-  
152 ing to the PM<sub>10.6</sub> mass fraction. Samples were collected at a flow rate of 6 L min<sup>-1</sup>. All flow rates were  
153 monitored by a thermal mass flow meter (TSI Inc., model 4140). These samples were also used to de-  
154 termine the elemental composition (including Fe) and the fraction of iron oxides in the total mass.

### 155 2.3. The Multi-Wavelength Absorbance Analyzer (MWAA)

156 The aerosol absorption coefficient,  $b_{\text{abs}}(\lambda)$ , at 5 wavelengths ( $\lambda = 375, 407, 532, 635$ , and 850 nm) was  
157 measured by *in situ* analysis of the quartz filter samples using the Multi-Wavelength Absorbance Ana-  
158 lyzer (MWAA), described in detail in Massabò et al. (2013; 2015).

159 The MWAA performs a non-destructive scan of the quartz filters on at 64 different points, each ~ 1 mm<sup>2</sup>  
160 wide. It measures the light transmission through the filter as well as backscattering at two different angles  
161 (125° and 165°). This is necessary to constrain the multiple scattering effects occurring within the par-  
162 ticle-filter system. The measurements are used as input of to a radiative transfer model (Hänel, 1987;  
163 1994) as implemented by Petzold and Schönlinner (2004) for the Multi-Angle Absorption Photometry  
164 (MAAP) measurements. In this model, a two stream approximation is applied (Coakley and Chylek,  
165 1975), in which the fractions of hemispherical backscattered radiation with respect to the total scattering  
166 for collimated and diffuse incident radiation are approximated on the basis of the Henyey-Greenstein  
167 scattering phase function (Hänel, 1987). This approximation assumes a wavelength-independent asym-  
168 metry parameter ( $g$ ) set to 0.75, appropriate for mineral dust (Formenti et al., 2011; Ryder et al., 2013b).

169 The total uncertainty, including the effects of photon counting and the deposit inhomogeneity, on the  
170 absorption coefficient measurement is estimated at 8% [\(Massabò et al., 2013\)](#).

## 171 **2.4. Gravimetric analysis**

172 The aerosol mass deposited on [the filters](#) ( $\mu\text{g}$ ) was obtained by weighing the quartz filter before and after  
173 sampling, after a period of 48 hours of conditioning in a room with controlled atmospheric conditions  
174 (temperature,  $T \sim 20 \pm 1 \text{ }^\circ\text{C}$ ; relative humidity,  $\text{RH} \sim 50 \pm 5\%$ ). Weighing is performed with an analyt-  
175 ical balance (Sartorius model MC5, precision of  $1 \mu\text{g}$ ), and repeated three times to control the statistical  
176 variability of the measurement. Electrostatic effects are removed by exposing the filters, prior weighing,  
177 to a de-ionizer. The error ~~on~~[in](#) the measured mass is estimated at  $1\theta \mu\text{g}$ , including the repetition varia-  
178 bility. The aerosol mass concentration ( $\mu\text{g m}^{-3}$ ) is obtained by dividing the mass deposited on [the filter](#)  
179 to the total volume of sampled air ( $\text{m}^3$ ) obtained from the mass flowmeter measurements [\(+5%\)](#). [The](#)  
180 [percent error on mass concentrations is estimated to 5%](#).

## 181 **2.5. Dust composition measurements**

### 182 **2.5.1. Elemental composition**

183 Elemental concentrations for the major constituents of mineral dust (Na, Mg, Al, Si, P, S, Cl, K, Ca, Fe,  
184 Ti, Mn) were obtained by ~~a~~-Wavelength Dispersive X-ray ~~fluorescence~~[Fluorescence](#) (WD-XRF) of the  
185 Nuclepore filters using a PW-2404 spectrometer by Panalytical. Excitation X-rays are produced by a  
186 Coolidge tube ( $I_{\text{max}} = 125 \text{ mA}$ ,  $V_{\text{max}} = 60 \text{ kV}$ ) with a Rh anode; [the](#) primary X-ray spectrum can be  
187 controlled by inserting filters (Al, at different thickness) between the anode and the sample. Each ele-  
188 ment was analyzed three times, with specific conditions (voltage, tube filter, collimator, analyzing crys-  
189 tal, and detector). Data collection was controlled by the SuperQ software provided with the instrument.  
190 The elemental mass thickness ( $\mu\text{g cm}^{-2}$ ), that is, the analyzed elemental mass per unit surface, was ob-  
191 tained by comparing the elemental yields with a sensitivity curve measured in the same geometry on a  
192 set of certified mono- or bi-elemental thin layer standards by Micromatter Inc. The certified uncertainty  
193 [of](#)~~the~~ standard deposit ( $\pm 5\%$ ) determines the lower limit [of](#)~~the~~ uncertainty [of](#)~~the~~ measured ele-  
194 mental concentrations, which ranges ~~between~~ [8% and 10%](#) depending on the [element](#) considered-~~ele-~~  
195 [ment](#). Thanks to the uniformity of the aerosol deposit on the filters, the atmospheric elemental concen-  
196 trations ( $\mu\text{g m}^{-3}$ ) were calculated by multiplying the analyzed elemental mass thickness by the ratio  
197 between the collection and analyzed surfaces of each sample (41 and 22 mm, respectively), then di-  
198 [viding](#)~~ed~~ by the total sampled volume ( $\text{m}^3$ ). Finally, concentrations of light-weight elements (atomic



199 number  $Z < 19$ ) were corrected for the underestimation induced by the self-absorption of the emitted  
200 soft X-rays inside aerosol particles according to Formenti et al. (~~2014~~2010).

201 Additional XRF analysis of the quartz filters ~~was~~ ~~has been~~ performed both in the PM<sub>10.6</sub> and the PM<sub>2.5</sub>  
202 fractions, ~~so~~ to verify the absence of biases between the experiments dedicated to the determination of  
203 particle composition ~~to~~ ~~and~~ those where the optical properties were measured.

### 204 2.6.2. Iron oxide content

205 The content and the mineralogical speciation of the iron oxides, also defined as free-iron, ~~that is i.e.~~, the  
206 fraction of iron ~~which~~ ~~that~~ is not in the crystal lattice of silicates (Karickhoff and Bailey, 1973), was  
207 determined by XANES (X-ray absorption near-edge structure) in the Fe K-range ( $K_{\alpha}$ , 7112 eV) at the  
208 SAMBA (Spectroscopies Applied to Materials based on Absorption) beamline at the SOLEIL synchro-  
209 tron facility in Saclay, France (Briois et al., 2011). The position and shape of the K pre-edge and edge  
210 peaks were analyzed as they depend on the oxidation state of iron and the atomic positions of the neigh-  
211 boring ions, mostly  $O^+$  and  $OH^-$ .

212 As in Formenti et al. (2014b), samples were mounted in an external setup mode. A Si(220) double-  
213 crystal monochromator was used to produce a monochromatic X-ray beam, which was 3000 x 250  $\mu\text{m}^2$   
214 in size at the focal point. The energy range was scanned from 6850 eV to 7800 eV at a step resolution  
215 varying between 0.2 eV in proximity to the Fe-K absorption edge (at 7112 eV) to 2 eV in the extended  
216 range. Samples were analyzed in fluorescence mode without prior preparation. One scan acquisition  
217 lasted approximately 30 minutes, and was repeated three times to improve the signal-to-noise ratio.

218 The same analytical protocol was applied to five standards of Fe(III)-bearing minerals (**Table 1**), includ-  
219 ing iron oxides (hematite, goethite) and silicates (illite, montmorillonite, nontronite). The standard spec-  
220 tra were used to deconvolute the dust sample spectra to quantify the mineralogical status of iron. The  
221 linear deconvolution ~~was~~, performed with the Athena IFEFFIT freeware analysis program (Ravel and  
222 Newville, 2005). ~~This~~, provided ~~with~~ the proportionality factors,  $\alpha_{i-}$ , representing the mass fraction of  
223 elemental iron to be assigned to the  $i$ -th standard mineral. In particular, the values of  $\alpha_{hem}$  and  $\alpha_{goe}$   
224 represent the mass fractions of elemental iron that can be attributed to hematite and goethite, and  $\alpha_{Fe\ ox}$   
225 ( $\alpha_{hem} + \alpha_{goe}$ ), the mass fraction of elemental iron that can be attributed to iron oxides.

### 226 2.6.3. Calculation of the iron oxide content



227 The measured elemental concentrations obtained by X-ray Fluorescence (XRF) are expressed in the  
 228 form of elemental oxides and summed to estimate the total mineral dust mass concentration  $MC_{dust}$  ac-  
 229 cording to the equation from Lide (1992)

230

$$231 \quad [MC_{dust}] = 1.12 \times \left\{ \begin{array}{l} 1.658[Mg] + 1.889[Al] + 2.139[Si] + 1.399[Ca] + 1.668[Ti] + 1.582[Mn] \\ + (0.5 \times 1.286 + 0.5 \times 1.429 + 0.47 \times 1.204)[Fe] \end{array} \right\} \quad (4)$$

232

233 The relative uncertainty ~~on~~ in  $MC_{dust}$ , estimated from the analytical error ~~in~~ the measured  
 234 concentrations, does not exceed 6%. [As it will be explained in the result section \(paragraph 3.1\), the](#)  
 235 [values of  \$MC\_{dust}\$  estimated from Equation 4 were found in excellent agreement with the measured](#)  
 236 [gravimetric mass on the filters.](#)

237 The fractional mass ratio (in percent) of elemental iron ( $MR_{Fe\%}$ ) with respect to the total dust mass con-  
 238 centration,  $MC_{dust}$ , is then calculated as

239

$$240 \quad MR_{Fe\%} = \frac{[Fe]}{[MC_{Dust}]} \times 100 \quad (5)$$

241

242 The mass concentration of iron oxides or free-iron ( $MC_{Fe\ ox}$ ), representing the fraction of elemental iron  
 243 in the form of hematite and goethite ( $Fe_2O_3$  and  $FeOOH$ , respectively), is equal to

244

$$245 \quad MC_{Fe\ ox} = MC_{hem} + MC_{goe} \quad (6)$$

246

247 where  $MC_{hem}$  and  $MC_{goe}$  are the total masses of hematite and goethite. These can be calculated from the  
 248 values  $\alpha_{hem}$  and  $\alpha_{goe}$  from XANES analysis, which represent the mass fractions of elemental iron at-  
 249 tributed to hematite and goethite, as

250

$$251 \quad MC_{hem} = \frac{\alpha_{hem} \times [Fe]}{0.70} \quad (7.a)$$

$$MC_{goe} = \frac{\alpha_{goe} \times [Fe]}{0.63} \quad (7.b)$$

where the values of 0.70 and 0.63 represent the mass molar fractions of Fe in hematite and goethite, respectively. The relative errors of  $MC_{hem}$  and  $MC_{goe}$  are obtained from the uncertainties of the values of  $\alpha_{hem}$  and  $\alpha_{goe}$  from XANES analysis (less than 10%).

The mass ratio of iron oxides ( $MR_{Fe\ ox\%}$ ) with respect to the total dust mass can then be calculated as

$$MR_{Fe\ ox\%} = MC_{Fe\ ox} \times MR_{Fe\ \%} \quad (8)$$

### 3. Experimental protocol

At the beginning of each experiment, the chamber was evacuated by to  $10^{-4}$ - $10^{-5}$  hPa. Then, the reactor was filled with a mixture of 80% N<sub>2</sub> and 20% O<sub>2</sub> at a pressure slightly exceeding the current atmospheric pressure, in order to avoid contamination from ambient air. The experiments were conducted at ambient temperature and at a relative humidity <2%. As in Di Biagio et al. (2014; 2016,2017), dust aerosols were generated by mechanical shaking of the parent soils, previously sieved to < 1000 μm and dried at 100 °C for about 1 h to remove any residual humidity. About 15 g of soil was placed in a Buchner flask and shaken for about 30 min at 100 Hz by means of a sieve shaker (Retsch AS200). The dust particles produced by the mechanical shaking, mimicking the saltation processing that soils experience when eroded by strong winds, as were then injected in the chamber by flushing the flask with N<sub>2</sub> at 10 L min<sup>-1</sup> for about 10-15 min, whilst continuing shaking the soil. Di Biagio et al. (2014; 2017) have demonstrated the realism of the generation system concerning the composition and the size distribution of the generated dust with respect to the properties of mineral dust in the atmosphere.

The dust was injected for about 10-15 minutes, and left remained suspended in the chamber for approximately 120 min thanks to the 4-wheel fan located in the bottom of the chamber body. Previous measurements at the top and bottom of the chamber showed that the fan ensures a homogeneous distribution of the dust starting approximately 10 minutes after the end of the injection (Di Biagio et al., 2014).

279 To compensate for the air extracted from the chamber by sampling, a particle-free flow of N<sub>2</sub>/O<sub>2</sub>, regu-  
280 lated in real time as a function of the total volume of sampled air, was re-injected in the chamber. To  
281 avoid excessive dilution the flow was limited to 20 L min<sup>-1</sup>. Two experiments per soil type were con-  
282 ducted: a first experiment for sampling on the nuclepore polycarbonate filters (determination of the ele-  
283 mental composition and the iron oxide fraction) and *in situ* measurements of the infrared optical con-  
284 stants (Di Biagio et al., 20162017), and a second experiment [sampling](#) on total quartz filter and impactor  
285 for the study of dust MAE presented in this paper.

286 **Figure 1** illustrates as typical example the time series of the aerosol mass concentration during the two  
287 experiments conducted for the Libyan sample. The comparison demonstrates the repeatability of the dust  
288 concentrations, both in absolute values and in temporal dynamics. It also shows that the mass concen-  
289 trations decreased very rapidly by gravitational settling within the first 30 minutes of the experiment  
290 (see also the discussion in Di Biagio et al., (20162017)), after which concentrations only decrease by  
291 dilution. The filter sampling was started after this transient phase, and then continued through the end of  
292 the experiments, in order to collect enough dust on [the filter membranes](#) for [subsequent the](#) chemical  
293 analysis. Blank samples were collected before the start of the experiments by placing the [loaded filter](#)  
294 holders [loaded with filter membranes](#) in line with the chamber and by flushing them for a few seconds  
295 with air coming from the chamber.

296 At the end of each experimental series with a given soil sample, the chamber was manually cleaned in  
297 order to remove carry-over caused by resuspension of particles deposited to the walls. Background con-  
298 centrations of aerosols in the chamber vary between 0.5 and 2.0 µg m<sup>-3</sup>, i.e., a factor of 500 to 1000  
299 below the operating conditions.

## 300 **34. Results and discussion**

301 The geographical location of the soil collection sites is shown in **Figure 2**, [whereas-and](#) the coordinates  
302 are summarized in **Table 2**. [As-discussed-in-Di-Biagio-et-al.\(2016\),the-selection-of-these-soils-and](#)  
303 [sediments-was-governed-by-the-need-of-representing-the-major-arid-and-semi-arid-regions-worldwide,](#)  
304 [the-need-of-taking-into-account-the-mineralogical-diversity-of-the-soil-composition-at-the-global-scale,](#)  
305 [and-finally-by-their-availability-in-sufficient-quantities-for-injection-in-the-chamber.](#) When doing so, we  
306 [obtained-a-set-of-twelve-samples-distributed-worldwide-but-mostly-in-Northern-and-Western-Africa](#)  
307 [\(Libya, Algeria, Mali, Bodélé\) and the Middle East \(Saudi Arabia and Kuwait\). Individual samples from](#)  
308 [the Gobi desert in Eastern Asia, the Namib Desert, the Strzelecki desert in Australia, the Patagonian](#)

309 ~~deserts in South America, and the Sonoran Desert in Arizona have also been investigated. The selection~~  
310 ~~of these soils and sediments was made out of 137 individual top-soil samples collected in major arid and~~  
311 ~~semi-arid regions worldwide and representing the mineralogical diversity of the soil composition at the~~  
312 ~~global scale. As discussed in Di Biagio et al. (2017), this large sample set was reduced byto a set of 19~~  
313 ~~samples representing the mineralogical diversity of the soil composition at the global scale and based on~~  
314 ~~their availability in sufficient quantities for injection in the chamber. Because some of the experiments~~  
315 ~~did not produce enough dust to perform good-quality optical measurements, in this paper we present a~~  
316 ~~set of twelve samples distributed worldwide but mostly from Northern and Western Africa (Libya,~~  
317 ~~Algeria, Mali, Bodélé) and the Middle East (Saudi Arabia and Kuwait). Individual samples from the~~  
318 ~~Gobi desert in Eastern Asia, the Namib Desert, the Strzelecki desert in Australia, the Patagonian deserts~~  
319 ~~in South America, and the Sonoran Desert in Arizona have were also been investigated.~~

#### 320 **3.1. Elemental composition and iron oxide content**

321 A total of 41 filters including 15 polycarbonate filters (12 samples and 3 blanks) and 25 quartz filters  
322 (12 for the total fraction, 10 for the fine fraction and 3 blanks) were collected for analysis.

323 The dust mass concentration found by gravimetric analysis varied between  $50 \mu\text{g m}^{-3}$  and  $5 \text{mg m}^{-3}$ , in  
324 relatively good agreement with the dust mass concentrations,  $MC_{dust}$ , from (Equation 4), based on ~~X-~~  
325 ~~ray Ray fluorescence FluorescenceXRF analysisaAnalysis~~: the slope of the linear regression between  
326 the calculated and the gravimetric values of  $MC_{dust}$  is 0.90 with  $R^2 = 0.86$ .

327 Di Biagio et al. (20162017) showed that clays are the most abundant mineral phases, together with quartz  
328 and calcite, and that significant variability exists as function of the compositional heterogeneity of the  
329 parent soils. Here we use the Fe/Ca and Si/Al elemental ratios obtained from ~~X-ray FluorescenceXRF~~  
330 analysis to discriminate the origin of ~~used~~ dust samples. These ratios have been extensively used in the  
331 past to discriminate the origin of African dust samples collected in the field (Chiapello et al., 1997;  
332 Formenti et al., 2011; Formenti et al., 2014a). The values obtained during our experiments are reported  
333 in **Table 3**. There is a very good correspondence between the values obtained for the Mali, Libya, ~~Al-~~  
334 ~~geria, Mauritania~~ and (to a lesser extent) Morocco experiments to values found in environmental aerosol  
335 samples by Chiapello et al. (1997) and Formenti et al. (2011; 2014a). ~~These authors indicate that dust~~  
336 ~~from local erosion of Sahelian soils, such as from Mali, have Si/Al ratios in the range of 2-2.5 and Fe/Ca~~  
337 ~~ratios in the range 3-20, depending on the time proximity to the erosion event. Dust from sources in the~~  
338 ~~Sahara, such as Libya and Algeria, show Si/Al ratios in the range of 2-3 and Fe/Ca ratios in the range~~

339 0.7-3, whereas dust from Morocco has Si/Al ratios around 3 and Fe/Ca ratios around 0.4. The only major  
340 difference is observed for the Bodélé experiment, for which the Fe/Ca ratio is enriched by a factor of 6  
341 with respect to the values of 1 found during ~~to~~ the field observations (Formenti et al., 2011; ~~Formenti et~~  
342 ~~al., 2014a~~). This could reflect the fact that the Bodélé aerosol in the chamber is generated from a sedi-  
343 ment sample and not from a soil. As a matter of fact, the Bodélé sediment sample ~~is constituted~~ consists  
344 of by a very fine powder which becomes very easily airborne. ~~Henceforth, and contrary to the soil sam-~~  
345 ~~ples, this~~ This powder is likely to be injected in the chamber with little or no size fractionation. ~~Hence-~~  
346 ~~forth, the aerosol generated from it~~ As a consequence, should have a closer ~~the~~ composition to the  
347 original powder of the aerosol collected in the chamber could reflect more that of the parent sedimentary  
348 soil than ~~the not the~~ other samples. On the other hand, Bristow et al. (2010) and Moskowitz et al. (2016)  
349 showed ed that the iron content and speciation of the Bodélé sediments is very heterogeneous at the source  
350 scale. For samples from areas other than ~~non-~~ northern African ~~samples~~, the largest variability is observed  
351 for the Fe/Ca values, ranging from 0.1 to 8, whereas the Si/Al ratio varied only between 2.5 and 4.8. In  
352 this case, values are available in the literature for comparison (e.g., Cornille et al., 1990; Reid et al.,  
353 1994; Eltayeb et al., 2001; Lafon et al., 2006; Shen et al., 2007; Radhi et al., 2010; 2011; Formenti et  
354 al., 2011; 2014a; Scheuvens et al., 2013, and references within). Values in the PM<sub>2.5</sub> fraction are very  
355 consistent with those obtained in the PM<sub>10.6</sub>: their linear correlation has a slope of 1.03 ( $\pm 0.05$ ) and a  $R^2$   
356 equal to 0.97, suggesting that the elemental composition is relatively size-independent.

357 The mass fraction of total Fe ( $MC_{Fe\%}$  from Equation 5), also reported in **Table 3**, ranged from 2.8 (Na-  
358 mibia) to 7.3% (Australia), ~~values found for the Namibia and the Australia samples, respectively. This~~  
359 These are in the range ~~is in good agreement with of~~ values reported in the literature, taking into account  
360 that differences might be also due to the method (direct measurement/calculation) and/or the size fraction  
361 over which the total dust mass concentration is estimated (Chiapello et al., 1997; Reid et al., 1994; 2003;  
362 Derimian et al., 2008; Formenti et al., 2001; 2011; 2014a; Scheuvens et al., 2013). The agreement of  
363  $MC_{Fe\%}$  values obtained by the XRF analysis of polycarbonate filters (Equation 5) and those obtained  
364 from the XRF analysis of the quartz filters, normalized to the measured gravimetric mass is well within  
365 10% (~~that is,~~ the percent error of each estimate). ~~An the e-~~ Exceptions are the samples ~~of from~~ Bodélé  
366 and Algeria, for which the values obtained from the analysis of the quartz filters are significantly lower  
367 than those obtained from the nuclepore filters (3.1% versus 4.1% for Bodélé and 4.3% versus 6.8% for  
368 Algeria). We treat that as an additional source of error in the rest of the analysis, and add it to the total  
369 uncertainty. In the PM<sub>2.5</sub> fraction, the content of iron is more variable, ranging from 4.4% (Morocco) to

370 33.6% (Mali), showing a size dependence. A word of caution on this conclusion ~~as is that~~ the two esti-  
371 mates are not necessarily consistent in the way that the total dust mass is estimated (from Equation 4 for  
372 the PM<sub>10.6</sub> fraction and by gravimetric weighing ~~for~~ the PM<sub>2.5</sub>).

373 Finally, between 11 and 47% of iron in the samples can be attributed to iron oxides, in variable propor-  
374 tions between hematite and goethite. The iron oxide fraction of total Fe in this study is ~~on~~ at the lower  
375 end of the range (36-72%) estimated for field dust samples of Saharan/Sahelian origin (Formenti et al.  
376 2014b). The highest value of Formenti et al. (2014b), obtained for a sample of locally-emitted dust col-  
377 lected at the Banizoumbou station in the African Sahel, is anyhow in excellent agreement with the value  
378 of 62% obtained for an experiment (not shown here) using a soil collected in the same area. Likewise,  
379 the proportions between hematite and goethite (not shown) are reproduced, showing that goethite is more  
380 abundant than hematite. The mass fraction of iron oxides ( $MR_{Fe\ ox\%}$ ), estimated from Equation 8 and  
381 shown in Table 3, ranges between 0.7% (Kuwait) ~~to~~ and 3.6% (Australia), which is in the range of  
382 available field estimates (Formenti et al., 2014a; Moskowitz et al., 2016). For China, our value of  $MR_{Fe\ ox\%}$   
383  $ox\%$  is lower by almost a factor of 3 ~~in comparison with~~ compared to that obtained on ~~the same~~ of the  
384 same origin sample by Alfaro et al. (2004) (0.9% against 2.8%), whereas on a sample from Niger (~~how-~~  
385 ~~ever~~ not considered in this study) our estimates and that by Alfaro et al. (2004) agree perfectly agree  
386 (5.8%). A possible underestimate of the iron oxide fraction for samples other than those from the Sahara-  
387 Sahel area could be due to the fact that - opposite to the experience of Formenti et al. (2014b) - the linear  
388 deconvolutions of the XANES spectra were not always satisfactory (see Figure S1 in the supplementary).  
389 This resulted in a significant residual between the observed and fitted XANES spectra. ~~Indeed~~ In fact,  
390 the mineralogical reference for hematite is obtained from a soil from Niger (Table 1) and might not be  
391 fully suitable for representing aerosols of different origins. Additional differences could arise from dif-  
392 ferences in the size distributions of the generated aerosol. As a matter of fact, the number fraction of  
393 particles in the size classes above 0.5  $\mu\text{m}$  in diameter is are different in the dust aerosol generated in the  
394 Alfaro et al. (2004) study ~~with respect compared~~ to ours. In the study by Alfaro et al. (2004), the number  
395 fraction of particles is lowest in the 0.5-0.7 size class and highest between 1 and 5  $\mu\text{m}$ . ~~On the contrary~~ In  
396 contrast, in our study the number fraction is lowest in the 1-2  $\mu\text{m}$  size range and highest between 0.5  
397 and 0.7  $\mu\text{m}$ . These differences could ~~yield~~ either be due to differences in the chemical composition  
398 and/or ~~to a difference~~ in the total mass in the denominator of Equation 8.

### 399 **34.2. Spectral and size -variability of the mass absorption efficiency**

400 The spectral mass absorption efficiency (MAE) at 375, 407, 532, 635, and 850 nm for the PM<sub>10.6</sub> and  
401 the PM<sub>2.5</sub> dust fractions are summarized in **Table 4** and displayed in **Figure 3**. Regardless of particle  
402 size, the MAE values decrease with increasing wavelength (almost one order of magnitude between 375  
403 and 850 nm), and display a larger variability at shorter wavelengths. The MAE values for the PM<sub>10.6</sub>  
404 range from  $37 (\pm 3) 10^{-3} \text{ m}^2 \text{ g}^{-1}$  to  $135 (\pm 11) 10^{-3} \text{ m}^2 \text{ g}^{-1}$  at 375 nm, and from  $1.3 (\pm 0.1) 10^{-3} \text{ m}^2 \text{ g}^{-1}$  to  $15$   
405  $(\pm 1) 10^{-3} \text{ m}^2 \text{ g}^{-1}$  at 850 nm. Maxima are found for the Australia and Algeria samples, whereas the minima  
406 are for Bodélé and Namibia, respectively at 375 and 850 nm. In the PM<sub>2.5</sub> fraction, the MAE values  
407 range from  $95 (\pm 8) 10^{-3} \text{ m}^2 \text{ g}^{-1}$  to  $711 (\pm 70) 10^{-3} \text{ m}^2 \text{ g}^{-1}$  at 375 nm, and from  $3.2 (\pm 0.3) 10^{-3} \text{ m}^2 \text{ g}^{-1}$  to  $36$   
408  $(\pm 3) 10^{-3} \text{ m}^2 \text{ g}^{-1}$  at 850 nm. Maxima at both 375 and 850 nm are found for the Morocco sample, whereas  
409 the minima are for Algeria and Namibia, respectively. The MAE values for mineral dust resulting from  
410 this work are ~~in~~ relatively in good agreement with the estimates available in the literature (Alfaro et al.,  
411 2004; Linke et al., 2006; Yang et al., 2009; Denjean et al., 2016), reported in **Table 5**. For the China  
412 Ulah Buhn sample, Alfaro et al. (2004) reported  $69.1 10^{-3}$  and  $9.8 10^{-3} \text{ m}^2 \text{ g}^{-1}$  at 325 and 660 nm, respec-  
413 tively. The former is lower than the value of  $99 10^{-3} \text{ m}^2 \text{ g}^{-1}$  that we obtain by extrapolating our measure-  
414 ment at 375 nm. Likewise, our values for the Morocco sample are higher than reported by Linke et al.  
415 (2006) at 266 and 660 nm. Conversely, the agreement with the estimates of Yang et al. (2009) for mineral  
416 dust locally re-suspended in Xianghe, near Beijing (China) is very good at all wavelengths between 375  
417 and 880 nm. As expected, the MAE values for mineral dust resulting from this work are almost one  
418 order of magnitude smaller than for other absorbing aerosols. For black carbon, MAE values are in the  
419 range of  $6.5\text{--}7.5 \text{ m}^2 \text{ g}^{-1}$  at 850 nm (Bond and Bergstrom, 2006; Massabò et al., 2016), and ~~vary-decrease~~  
420 in a linear way with the logarithm of the ~~inversely with~~ wavelength. For brown carbon, the reported  
421 MAE range between  $2.3\text{--}7.0 \text{ m}^2 \text{ g}^{-1}$  at 350 nm (Chen and Bond, 2010; Kirchstetter et al., 2004; Massabò  
422 et al., 2016),  $0.05\text{--}1.2 \text{ m}^2 \text{ g}^{-1}$  at 440 nm (Wang et al., 2016) and  $0.08\text{--}0.72 \text{ m}^2 \text{ g}^{-1}$  at 550 nm (Chen and  
423 Bond, 2010).

424 The analysis of **Table 4** indicates that, at every wavelength, the MAE values in the PM<sub>2.5</sub> fraction are  
425 equal or higher than those for PM<sub>10.6</sub>. The PM<sub>2.5</sub>/PM<sub>10.6</sub> MAE ratios reach values of 6 for the Mali sam-  
426 ple, but are mostly in the range 1.5-3 for the ~~remaining-other~~ aerosols. The vValues decrease with wave-  
427 length up to 635 nm, whereas at 850 nm they have values comparable to those at 375 nm. The observed  
428 size ~~-~~dependence of the MAE values is consistent with the expected behavior of light absorption of  
429 particles in the Mie and geometric optical regimes that ~~concern-are relevant for~~ the two size fractions.  
430 Light ~~-~~absorption of particles of sizes s smaller or equivalent to the wavelength is proportional to their



431 bulk volume, whereas for larger particles absorption occurs on their surface only (Bohren and Huffmann,  
432 1983). On the other hand, the size-resolved measurements of Lafon et al. (2006) show that the proportion  
433 (by volume) of iron oxides might be higher in the coarse than in the fine fraction, which would counteract  
434 the size-dependence behavior of MAE. To validate the observations, we calculated the spectrally-re-  
435 solved MAE values in the two size fractions using the Mie code for homogeneous spherical particles  
436 (Bohren and Huffmann, 1983) and the number size distribution estimated by (Di Biagio et al.,  
437 [2016\(2017\)](#)) and averaged over the duration of filter sampling. We estimated the dust complex refractive  
438 index as a volume-weighted average of a non-absorbing dust fraction having the refractive index of  
439 kaolinite, [the](#) dominant mineral in our samples (see Di Biagio et al., [20162017](#)), from Egan et Hilgeman  
440 (1979) and an absorbing fraction estimated from the mass fraction of iron oxides and having the refrac-  
441 tive index of hematite (Bedidi and Cervelle, 1993). [The r](#)Results of this calculation indicate that the  
442 observed size-[dependent](#) behavior is well reproduced at all wavelengths, even in the basic hypothesis  
443 that the mineralogical composition does not change with size. The only exception is 850 nm, where at  
444 times, PM<sub>2.5</sub>/PM<sub>10.6</sub> MAE ratio is much higher than expected theoretically. We attribute that to the rela-  
445 tively high uncertainty affecting the absorbance measurements at this wavelength, where the signal-to-  
446 noise ratio is low. Indeed, the two sets of values (MAE in the PM<sub>2.5</sub> fraction and MAE in the PM<sub>10.6</sub>  
447 fraction) are not statistically different according to a two-pair t-test (0.01 and 0.05 level of confidence),  
448 confirming that any attempt of differentiation [of](#) the size-[dependence](#) at this wavelength would require  
449 a stronger optical signal.

450 The analysis of the spectral dependence, using [a-the](#) power-law function fit [as-\(from](#) Equation 2), pro-  
451 vides [with](#) the values of the Angstrom Absorption Exponent (AAE), also reported in **Table 4**. Contrary  
452 to the MAE values, there is no statistically significant size-[dependence](#) of the AAE values, ranging from  
453 2.5 ( $\pm 0.2$ ) to 4.1 ( $\pm 0.3$ ), with an average of 3.3 ( $\pm 0.7$ ), for the PM<sub>10.6</sub> size fraction and between 2.6 ( $\pm$   
454 0.2) and 5.1 ( $\pm 0.4$ ), with an average of 3.5 ( $\pm 0.8$ ), for the PM<sub>2.5</sub> fraction. Our values are in the range of  
455 those published in the [open](#)-literature (Fialho et al., 2005; Linke et al., 2006; Müller et al., 2009; Petzold  
456 et al., 2009; Yang et al., 2009; Weinzierl et al., 2011; Moosmüller et al., 2012; Denjean et al., 2016),  
457 shown in **Table 5**. AAE values close to 1.0 are found for urban aerosols where fossil fuels combustion  
458 is dominant, while AAE values for brown carbon (BrC) from incomplete combustion are in the range  
459 3.5-4.2 (Yang et al., 2009; Chen et al., 2015; Massabò et al., 2016).

460 Finally, **Figure 4** shows correlations between [the](#) MAE values in the PM<sub>10.6</sub> fraction (Figure [34.a](#)) and  
461 in the PM<sub>2.5</sub> fraction (Figure [34.b](#)) and the estimated percent mass fraction of iron and iron oxides

462 ( $MC_{Fe\%}$  and  $MC_{Fe\ ox\%}$ ), respectively. Regardless of the size fraction, ~~t~~The correlation between the MAE  
463 values and the percent mass of total elemental iron are ~~satisfactory~~. ~~Higher higher correlations are ob-~~  
464 ~~tained~~ at 375, 407 and 532 nm, ~~and in the  $PM_{2.5}$  fraction, where a linear correlation with  $R^2$  up to 0.94~~  
465 ~~are obtained~~. Best correlations are obtained when forcing the intercept to zero, indicating that elemental  
466 iron fully accounts for the measured absorption. At these wavelengths, linear correlations with the mass  
467 fraction of iron oxides are ~~loose~~ low in the  $PM_{10.6}$  mass fraction ( $R^2$  up to 0.38-0.62), but ~~again satisfac-~~  
468 ~~tory~~ higher in the  $PM_{2.5}$  fraction ( $R^2$  up to 0.83-0.99), where, ~~whenever~~ however, one should keep in mind  
469 that they have been established only indirectly by considering the ratio of iron oxides to elemental iron  
470 independent of size. At 660 and 850 nm, little or no robust correlations ~~are is~~ obtained, often ~~based~~ on  
471 very few data points and with very low MAE values. It is noteworthy that, in both size fractions, the  
472 linear correlation yields a non-zero intercept ~~is obtained~~, indicating ~~a contribution from minerals~~ other  
473 ~~minerals but~~ than iron oxides ~~account to~~ for the measured absorption.

#### 474 **4.5. Conclusive remarks**

475 In this paper, we reported ~~new~~ laboratory measurements of the shortwave mass absorption efficiency  
476 (MAE) of mineral dust of different origins and as a function of size and wavelength in the 375-850 nm  
477 range. ~~Results~~ Our results ~~have been~~ were obtained in the CESAM simulation chamber using ~~generated~~  
478 mineral dust ~~generated~~ from natural parent soils, ~~in combination with~~ and optical and gravimetric anal-  
479 ysis on extracted samples.

480 Our results can be summarized as follows: at 375 nm, the MAE values are lower for the  $PM_{10.6}$  mass  
481 fraction (range 37-135  $10^{-3} \text{ m}^2 \text{ g}^{-1}$ ) than for the  $PM_{2.5}$  ~~fraction~~ (range 95-711  $10^{-3} \text{ m}^2 \text{ g}^{-1}$ ), and vary oppo-  
482 site to wavelength as  $\lambda^{-AAE}$ , where AAE (Angstrom Absorption Exponent) averages between 3.3-3.5  
483 regardless of size fraction. These results deserve some ~~conclusive~~ concluding comments:

- 484 • The size ~~-~~dependence, ~~yielding~~ characterized by significantly higher MAE values in the fine  
485 fraction ( $PM_{2.5}$ ) than ~~for the~~ in the bulk ( $PM_{10.6}$ ) aerosol, indicates that light ~~-~~absorption by min-  
486 eral dust can be important even during atmospheric transport over heavil~~y~~ polluted regions, ~~when~~  
487 ~~where~~ dust concentrations are significantly lower than at emission. This can be shown by com-  
488 paring the aerosol absorption optical depth (AAOD) at 440 nm for China, a well-known mixing  
489 region of mineral dust and pollution (e.g., Yang et al., 2009; Laskin et al., 2014; Wang et al.,  
490 2013), ~~as well as offshore western Africa where large urban centers are downwind of dust~~  
491 ~~transport areas~~ (Petzold et al., 2011). Laskin et al. (2014) reports that the average AAOD in ~~China~~

492 ~~the area~~ is of the order of 0.1; for carbonaceous absorbing aerosols (sum of black and brown  
493 carbon; [Andreae and Gelencsér, 2006](#)). This is lower or comparable to the AAOD of 0.17 and  
494 0.11 at 407 nm (~~fine and~~ total ~~and fine~~ mass fractions, respectively) that we ~~obtain~~ derive by a  
495 simple calculation ( $AAOD = MAE \times MC_{dust} \times H$ ), ~~where from~~ MAE ~~are the~~ values estimated in  
496 this study, ~~( $MC_{dust}$ )~~ the dust mass concentrations typically observed in ~~the area~~ urban area of  
497 [Beijing](#) during dust storms (Sun et al., ~~2004~~2005), and  $H$ , a scale height factor of 1 km).

498 • The spectral variability of the dust MAE values, represented by the AAE parameter, is equal in  
499 the PM<sub>2.5</sub> and PM<sub>10.6</sub> mass fractions. This suggests that, for a given size distribution, the possible  
500 variation of dust composition with size ~~does~~ not affect in a significant way the spectral behavior  
501 of the absorption properties. Our average value for AAE is  $3.3 \pm 0.7$ , higher than for black carbon,  
502 but in the same range ~~than as~~ light-absorbing organic (brown) carbon. As a result, depending on  
503 the environment, there can be some ambiguity in apportioning the AAOD based on spectral de-  
504 pendence. Bahadur et al. (2012) and Chung et al. (2012) couple the AAE and the spectral de-  
505 pendence of the total AOD (~~and/or its scattering fraction only~~) to overcome this problem. Still,  
506 Bahadur et al. (2012) show that there is an overlap in the scatterplots of the spectral dependence  
507 of the scattering and absorption fractions of the AOD based on ~~an~~ analysis of ground-based re-  
508 mote sensing data for mineral dust, urban, and non-urban fossil fuel over California. A closer  
509 look ~~should be taken at~~ observations in mixing areas where biomass burning ~~aerosols may~~  
510 have different chemical composition and/or mineral dust has heavy loadings ~~should be given~~ in  
511 order to generalize the clear separation observed in the spectral dependences of mineral dust and  
512 biomass burning (Bahadur et al., 2012). This aspect is relevant to the development of remote  
513 sensing ~~retrievals~~ of light-~~absorption by~~ aerosols from space, and their assimilation in climate  
514 models (Torres et al., 2007; Buchard et al., 2015; Hammer et al., 2016).

515 • There is an important sample-to-sample variability in our dataset of MAE values for mineral dust  
516 aerosols. At 532 nm, our ~~estimated average~~ MAE ~~values average to are at~~  $34 \pm 14 \text{ m}^2 \text{ g}^{-1}$  and  $78$   
517  $\pm 70 \text{ m}^2 \text{ g}^{-1}$  in the PM<sub>10.6</sub> and PM<sub>2.5</sub> mass fractions, respectively. Figure 3, showing the correlation  
518 with the estimated mass fraction of elemental iron and iron oxides, suggests that this variability  
519 could be related to the regional differences of the mineralogical composition of the parent soils.  
520 These observations lead to ~~different considerations~~ further conclusions. To start with, our study  
521 reinforces the need for regionally-resolved representation of the light-~~absorption~~ properties of

522 mineral dust in order to improve the representation of its effect on climate. As a matter of fact,  
523 the natural variability of the absorption properties that we obtain from our study is in the range  
524 50-100%, even when we limit ourselves to smaller spatial scales, for example those ~~of from~~ north  
525 Africa (samples from Libya, Algeria, Mali and Bodélé). ~~This is far above the  $\pm 5\%$  sensitivity~~  
526 ~~factor used by Solmon et al. (2008) to vary the single scattering albedo (as a proxy of absorption)~~  
527 ~~of mineral dust over western Africa, and to show how this could drastically change the climate~~  
528 ~~response in the region. As a comparison, Solmon et al. (2008) showed that varying the single~~  
529 ~~scattering albedo of mineral dust over western Africa by  $\pm 5\%$ , that is, varying the co-albedo (or~~  
530 ~~absorption) by 45% ( $0.1 \pm 0.045$ ) could drastically change the climate response in the region.~~

531 The question is then “how to represent this regional variability?” ~~As Like~~ Moosmüller et al.  
532 (2012) ~~and Engelbrecht et al. (2016)~~, we found that elemental iron is a very good proxy for the  
533 MAE, especially in the PM<sub>2.5</sub> fraction, where iron-bearing absorbing minerals (hematite, goe-  
534 thite, illite, smectite clays) ~~would beare~~ more concentrated. In the coarse fraction, Ca-rich min-  
535 erals, quartz, and feldspars could also play a role, and that could result in the observed lower~~ed~~  
536 correlation (although adding a term proportional to elemental Ca does not ~~ameliorate-improve~~  
537 the ~~correlation-result~~ in the present study). The correlation of the spectral MAE values with the  
538 iron oxide fraction is satisfactory but rather noisy, also owing to some uncertainty in the quanti-  
539 fication of iron oxides from X-Ray ~~Absorption-absorption~~ measurements. In this case, the inter-  
540 cept is significantly different from zero, again indicating that a small but ~~clear-distinct~~ fraction  
541 of absorption is due to minerals other than iron oxides. There are contrasting results on this topic:  
542 Alfaro et al. (2004) found an excellent correlation between MAE and the iron oxide content,  
543 whereas Klaver et al. (2011) found that the single scattering albedo (representing the capacity of  
544 an aerosol population to absorb light ~~with respect in relation~~ to extinction) was almost independ-  
545 ent on the mass fraction of iron oxides. Moosmüller et al. (2012) disagreed, pointing out ~~to~~ the  
546 uncertainty in the correction procedure of the measurement of absorption by Klaver et al. (2011).  
547 As a matter of fact, Klaver et al. (2011) and Alfaro et al. (2004) used the same correction proce-  
548 dure. It is more likely that the lack of correlation found in Klaver et al. (2011) is due to the fact  
549 that ~~other~~ minerals ~~other~~ than iron oxides contribute to absorption, in particular at their working  
550 wavelength (567 nm), where the absorption efficiency of iron oxides starts to weaken. Clearly,  
551 the linear correlation between elemental iron in mineral dust and its light-absorption properties

552 could ease the application and validation of climate models that [are](#) now starting [to include in-](#)  
553 [cluding](#) the representation of the mineralogy (Perlwitz et al., 2015a; 2015b; Scanza et al., 2015).  
554 Also, [they-this](#) would facilitate detecting source regions based on remote sensing of dust absorp-  
555 tion in the UV-VIS spectral region (e.g., Hsu et al., 2004). However, such a quantitative relation-  
556 ship cannot [be](#) uniquely determined from these studies, including the present one, which use  
557 different ways of estimating elemental iron, iron oxides, and the total dust mass. A more robust  
558 estimate should be obtained [fromby estimating](#) the imaginary parts of the complex refractive  
559 indices associated [to-with](#) these measurements of absorption, and their dependence on the min-  
560 eralological composition.

### 561 **Author contributions**

562 L. Caponi, P. Formenti, D. Massabò, P. Prati, C. Di Biagio, and J. F. Doussin designed the chamber  
563 experiments and discussed the results. L. Caponi and C. Di Biagio [realized-conducted](#) the experiments  
564 with contributions by M. Cazaunau, E. Pangui, P. Formenti, and J.F. Doussin. L. Caponi, D. Massabò  
565 and P. Formenti performed the full data analysis with contributions by C. Di Biagio, P. Prati and J.F.  
566 Doussin. L. Caponi, P. Formenti and S. Chevallier performed the XRF measurements. P. Formenti and  
567 G. Landrot performed the XAS measurements. D. Massabò performed the MWAA and the gravimetric  
568 measurements. M. O. Andreae, K. Kandler, T. Saeed, S. Piketh, D. Seibert, and E. Williams collected  
569 the soil samples used for experiments. L. Caponi, P. Formenti, D. Massabò and P. Prati wrote the man-  
570 uscript with comments from all co-authors.

### 571 **Acknowledgements**

572 [The RED-DUST project was supported by the French national programme LEFE/INSU, by the EC](#)  
573 [within the I3 project “Integration of European Simulation Chambers for Investigating Atmospheric Pro-](#)  
574 [cesses” \(EUROCHAMP 2020, grant agreement n. 730997\), by the Institut Pierre Simon Laplace \(IPSL\),](#)  
575 [and by OSU-EFLUVE \(Observatoire des Sciences de l’Univers-Enveloppes Fluides de la Ville à l’Ex-](#)  
576 [obiologie\) through dedicated research funding. This work has received funding from the European Un-](#)  
577 [ion’s Horizon 2020 research and innovation programme through the EUROCHAMP-2020 Infrastructure](#)  
578 [Activity under grant agreement no. 730997. It was supported by the French national programme](#)  
579 [LEFE/INSU, by the OSU-EFLUVE \(Observatoire des Sciences de l’Univers-Enveloppes Fluides de la](#)  
580 [Ville à l’Exobiologie\) through dedicated research funding, by the CNRS-INSU by supporting CESAM](#)  
581 [as national facility, and by the project of the TOSCA program of the CNES \(Centre National des Etudes](#)

582 [Spatiales](#)). C. Di Biagio was supported by the CNRS via the Labex L-IPSL. M. O. Andreae was sup-  
583 ported [by funding from King Saud University and the Max Planck Society](#)~~by the Max Society and by~~  
584 [King Saud University](#). The mobility of researchers between Italy and France was supported by the PICS  
585 programme MedMEx of the CNRS-INSU. The authors acknowledge the CNRS-INSU for supporting  
586 CESAM as national facility. K. Kandler acknowledges support from the Deutsche Forschungsgemein-  
587 schaft (DFG grant KA 2280/2-1). [The authors strongly thank the LISA staff who participated in the](#)  
588 [collection of the soil samples from Patagonia and the Gobi desert used in this study, and the two anon-](#)  
589 [ymous reviewers for useful comments on the manuscript. P. Formenti thanks Dr. Hans Moosmüller](#)  
590 [\(Desert Research Institute, Reno, Nevada\) for providing with fruitful](#) ~~elements~~[suggestions for-of im-](#)  
591 [provement and discussion to the paper.](#)

## 592 **References**

- 593 Alfaro, S. C., Lafon, S., Rajot, J. L., Formenti, P., Gaudichet, A., and Maille, M., Iron oxides and light  
594 absorption by pure desert dust: An experimental study, *J. Geophys. Res. Atmos.*, 109, D08208,  
595 doi:10.1029/2003JD004374, 2004.
- 596 [Andreae, M. O., and Gelencsér, A., Black carbon or brown carbon? The nature of light-absorbing car-](#)  
597 [bonaceous aerosols: \*Atmos. Chem. Phys.\*, 6, 3131-3148, 2006.](#)
- 598 [Anderson, T. L. and Ogren, J. A., Determining aerosol radiative properties using the TSI 3563 integrat-](#)  
599 [ing nephelometer, \*Aerosol. Sci. Technol.\*, 29, 57–69, 1998.](#)
- 600 [Andrews, E., Sheridan, P. J., Fiebig, M., McComiskey, A., Ogren, J. A., Arnott, P., Covert, D., Elleman,](#)  
601 [R., Gasparini, R., Collins, D., Jonsson, H., Schmid, B., and Wang J., Comparison of methods](#)  
602 [for deriving aerosol asymmetry parameter, \*J. Geophys. Res.\*, 111, D05S04,](#)  
603 [doi:10.1029/2004JD005734, 2006.](#)
- 604 [Arnott, W., Hamasha, K., Moosmüller, H., Sheridan, P. J., and Ogren, J. A., Towards aerosol light-](#)  
605 [absorption measurements with a 7 wavelength aethalometer: Evaluation with a photoacoustic](#)  
606 [instrument and 3 wavelength nephelometer, \*Aerosol Sci Tech.\*, 39\(1\), 17–29, 2005.](#)
- 607 Bahadur, R., P. S. Praveen, Y. Xu, and V. Ramanathan, Solar absorption by elemental and brown carbon  
608 determined from spectral observations, *PNAS*, 109(43), 17366-17371, 2012.
- 609 Balkanski, Y., Schulz, M., Claquin, T., and Guibert, S., Re-evaluation of Mineral aerosol radiative forc-  
610 ing suggests a better agreement with satellite and AERONET data, *Atmos. Chem. Phys.*, 7, 81–  
611 95, doi:10.5194/acp-7-81-2007, 2007.
- 612 Bedidi, A., and Cervelle B., Light scattering by spherical particles with hematite and goethitelike optical  
613 properties: Effect of water impregnation, *J. Geophys. Res.*, 98(B7), 11941–11952,  
614 doi:10.1029/93JB00188, 1993.
- 615 Bond, T.C. and Bergstrom, R.W., Light absorption by carbonaceous particles: an investigative review.  
616 *Aerosol Sci. Technol.* 40, 27e67, 2006.



- 617 Boucher, O., Randall, D., Artaxo, P., Bretherton, C., Feingold, G., Forster, P., Kerminen, V.-M., Kondo,  
618 Y., Liao, H., Lohmann, U., Rasch, P., Satheesh, S.K., Sherwood, S., Stevens B., and Zhang X.  
619 Y., Clouds and Aerosols. In: Climate Change 2013: The Physical Science Basis. Contribution of  
620 Working Group I to the Fifth Assessment Report of the Intergovernmental Panel on Climate  
621 Change [Stocker, T.F., D. Qin, G.-K. Plattner, M. Tignor, S.K. Allen, J. Boschung, A. Nauels,  
622 Y. Xia, V. Bex and P.M. Midgley (eds.)]. Cambridge University Press, Cambridge, United King-  
623 dom and New York, NY, USA, 2013.
- 624 Brégonzio-Rozier, L., F. Siekmann, C. Giorio, E. Pangui, S. B. Morales, B. Temime-Roussel, Aline  
625 Gratien, V. Michoud, S. Ravier, A. Tapparo, A. Monod, Jean-Francois Doussin, Gaseous prod-  
626 ucts and secondary organic aerosol formation during long term oxidation of isoprene and meth-  
627 acrolein, *Atmos. Chem. Phys.*, 15, 2953-2968, 2015.
- 628 Brégonzio-Rozier L., C. Giorio, F. Siekmann, E. Pangui, S. B. Morales, B. Temime-Roussel, A. Gratien,  
629 V. Michoud, M. Cazaunau, H. L. DeWitt, A. Tapparo, A. Monod and J.-F. Doussin, Secondary  
630 Organic Aerosol formation from isoprene photooxidation during cloud condensation-evaporation  
631 cycles, *Atmospheric Chemistry and Physics*, 16: 1747-1760, 2016.
- 632 Bristow, C. S., Hudson-Edwards, K. A., and Chappell, A.: Fertilizing the Amazon and equatorial Atlan-  
633 tic with West African dust, *Geophys. Res. Lett.*, 37, L14807, 10.1029/2010GL043486, 2010.
- 634 Buchard, V., da Silva, A. M., Colarco, P. R., Darmenov, A., Randles, C. A., Govindaraju, R., Torres,  
635 O., Campbell, J., and Spurr, R.: Using the OMI aerosol index and absorption aerosol optical  
636 depth to evaluate the NASA MERRA Aerosol Reanalysis, *Atmos. Chem. Phys.*, 15, 5743–5760,  
637 doi:10.5194/acp-15-5743-2015, 2015.
- 638 Chen, L.-W.A., Chow, J.C., Wang, X.L., Robles, J.A., Sumlin, B.J., Lowenthal, D.H., Zimmermann, R.,  
639 Watson, J.G., Multi-wavelength optical measurement to enhance thermal/optical analysis for car-  
640 bonaceous aerosol, *Atmos. Meas. Tech.* 8, 451-461, 2015.
- 641 Chen, Y. and Bond, T. C., Light absorption by organic carbon from wood combustion, *Atmos. Chem.*  
642 *Phys.*, 10:1773–1787, 2010.
- 643 [Chiapello, I., G. Bergametti, B. Chatenet, P. Bousquet, F. Dulac, and E. Santos Soares, Origins of Afri-  
644 can dust transported over the northeastern tropical Atlantic., \*J. Geophys. Res.\*, 102\(D12\), 13701-  
645 13709, 1997.](#)
- 646 Chiapello, I., Dust Observations and Climatology, in P. Knippertz and J.-B.W. Stuut (eds.), *Mineral  
647 Dust: A Key Player in the Earth System*, DOI 10.1007/978-94-017-8978-3\_\_7, ©Springer Sci-  
648 enceCBusiness Media, Dordrecht, 2014.
- 649 Chung, C. E., V. Ramanathan, and D. Decremer, Observationally constrained estimates of carbonaceous  
650 aerosol radiative forcing, *PNAS*, 109(29), 11624-11629, 2012.
- 651 Coakley, J.A. and Chylek, P., The two-stream approximation in radiative transfer: Including the angle  
652 of incident radiation, *J. Atmos. Sci.* 32, 409 – 418, 1975.
- 653 Colarco, P. R., O. B. Toon, O. Torres, and F. J. Rasch, Determining the UV imaginary part of refractive  
654 index of Saharan dust particles from TOMS data and a three dimensional model of dust transport,  
655 *J. Geophys. Res.*, 107(D16), 10.1029/2001JD000903, 2002.



- 656 [Collaud Coen, M., Weingartner, E., Apituley, A., Ceburnis, D., Fierz-Schmidhauser, R., Flentje, H.,](#)  
657 [Henzing, J.S., Jennings, S.G., Moerman, M., Petzold, A., Schmid, O., Baltensperger, U., Mini-](#)  
658 [mizing light absorption measurement artifacts of the Aethalometer: evaluation of five correction](#)  
659 [algorithms, Atmos. Meas. Tech. 3, 457-474, 2010.](#)
- 660 Denjean, C., Paola Formenti, Benedicte Picquet-Varrault, Edouard Pangui, Pascal Zapf, Y. Katrib, C.  
661 Giorio, A. Tapparo, A. Monod, B. Temime-Roussel, P. Decorse, C. Mangeney, Jean-Francois  
662 Doussin, Relating hygroscopicity and optical properties to chemical composition and structure  
663 of secondary organic aerosol particles generated from the ozonolysis of  $\alpha$ -pinene, Atmos. Chem.  
664 Phys., 15, 3339-3358, 2015a.
- 665 Denjean, C., Paola Formenti, Benedicte Picquet-Varrault, Marie Camredon, Edouard Pangui, Pascal  
666 Zapf, Katrib, Y., Giorio, C., Tapparo, A., Temime-Roussel, B., Monod, A., Bernard Aumont,  
667 Jean-Francois Doussin, Aging of secondary organic aerosol generated from the ozonolysis of  $\alpha$ -  
668 pinene: effects of ozone, light and temperature, Atmos. Chem. Phys., 15, 883-897,  
669 doi:10.5194/acp-15-883-2015, 2015b.
- 670 Denjean, C., Cassola, F., Mazzino, A., Triquet, S., Chevaillier, S., Grand, N., Bourriane, T., Mom-  
671 boisse, G., Sellegri, K., Schwarzenbock, A., Freney, E., Mallet, M., and Formenti, P., Size distri-  
672 bution and optical properties of mineral dust aerosols transported in the western Mediterranean,  
673 Atmos. Chem. Phys., 15, 21607–21669, doi:10.5194/acpd-15-21607-2015, 2015c.
- 674 Denjean, C., *et al.*, Size distribution and optical properties of African mineral dust after intercontinental  
675 transport, J. Geophys. Res. Atmos., 121, 7117–7138, doi:10.1002/2016JD024783, 2016.
- 676 Derimian, Y., A. Karnieli, Y. J. Kaufman, M. O. Andreae, T. W. Andreae, O. Dubovik, W. Maenhaut,  
677 and I. Koren: The role of iron and black carbon in aerosol light absorption. Atmos. Chem. Phys.,  
678 8, 3623–3637, (2008).
- 679 Di Biagio, C., Formenti P., Styler S. A., Pangui E., and Doussin J.-F., Laboratory chamber measurements  
680 of the longwave extinction spectra and complex refractive indices of African and Asian mineral  
681 dusts, Geophys. Res. Lett., 41, 6289-6297, doi:10.1002/2014GL060213, 2014.
- 682 [Di Biagio, C., Formenti, P., Balkanski, Y., Caponi, L., Cazaunau, M., Pangui, E., Journet, E., Nowak, S., Ca-](#)  
683 [quineau, S., Andreae, M. O., Kandler, K., Saeed, T., Piketh, S., Seibert, D., Williams, E., and Doussin,](#)  
684 [J.-F.: Global scale variability of the mineral dust long-wave refractive index: a new dataset of in situ](#)  
685 [measurements for climate modeling and remote sensing, Atmos. Chem. Phys., 17, 1901-1929,](#)  
686 [doi:10.5194/acp-17-1901-2017, 2017.](#)
- 687 [Di Biagio, C., Formenti, P., Balkanski, Y., Caponi, L., Cazaunau, M., Pangui, E., Journet, E., Nowak,](#)  
688 [S., Caquineau, S., Andreae, M. O., Kandler, K., Saeed, T., Piketh, S., Seibert, D., Williams, E.,](#)  
689 [and Doussin, J.-F.: Global scale variability of the mineral dust longwave refractive index: a new](#)  
690 [dataset of in situ measurements for climate modelling and remote sensing, Atmos. Chem. Phys.](#)  
691 [Discuss., doi:10.5194/acp-2016-616, in review, 2016.](#)
- 692 Dubovik, O., B. N. Holben, T. F. Eck, A. Smirnov, Y. J. Kaufman, M. D. King, D. Tanre, and I. Slutsker,  
693 Variability of absorption and optical properties of key aerosol types observed in worldwide lo-  
694 cations, J. Atmos. Sci., 59, 590–608, 2002.
- 695 Egan, W. G. and Hilgeman, T. W.: Optical Properties of Inhomogeneous Materials: Applications to  
696 Geology, Astronomy, Chemistry, and Engineering, Academic Press, 235 pp., 1979.

- 697 [Engelbrecht, J. P., Moosmüller, H., Pincock, S., Jayanty, R. K. M., Lersch, T., and Casuccio, G.: Technical note:](#)  
698 [Mineralogical, chemical, morphological, and optical interrelationships of mineral dust re-suspensions,](#)  
699 [Atmos. Chem. Phys., 16, 10809-10830, doi:10.5194/acp-16-10809-2016, 2016.](#)
- 700 Fialho, P., A.D.A. Hansen, R.E. Honrath, Absorption coefficients by aerosols in remote areas: a new  
701 approach to decouple dust and black carbon absorption coefficients using seven-wavelength Ae-  
702 thalometer data, *J. Aeros. Sci.*, 36, 267–282, 2005.
- 703 ~~[Filep, Á., Ajtai, T., Utry, N., Pintér, M., Nyilas, T., Takács, S., Máté, Z., Gelencsér, A., Hoffer, A.,](#)~~  
704 ~~[Schnaiter, M., Bozóki, Z., and Szabó, G., Absorption spectrum of ambient aerosol and its corre-](#)~~  
705 ~~[lation with size distribution in specific atmospheric conditions after a Red Mud Accident, \*Aero-\*](#)~~  
706 ~~[sol Air Qual. Res.](#)~~ 13, 49–59, 2013.
- 707 Formenti, P., S. Nava, P. Prati, S. Chevaillier, A. Klaver, S. Lafon, F. Mazzei, G. Calzolari, and M. Chiari,  
708 Self-attenuation artifacts and correction factors of light element measurements by X-ray analysis:  
709 Implication for mineral dust composition studies, *J. Geophys. Res.*, 115, D01203,  
710 doi:10.1029/2009JD012701, 2010.
- 711 Formenti, P., Rajot, J. L., Desboeufs, K., Saïd, F., Grand, N., Chevaillier, S., and Schmechtig, C., Air-  
712 borne observations of mineral dust over western Africa in the summer Monsoon season: spatial  
713 and vertical variability of physico-chemical and optical properties, *Atmos. Chem. Phys.*, 11,  
714 6387–6410, doi:10.5194/acp-11-6387-2011, 2011.
- 715 Formenti, P., Caquineau, S., Desboeufs, K., Klaver, A., Chevaillier, S., Journet, E. and Rajot, J. L.,  
716 Mapping the physico-chemical properties of mineral dust in western Africa: mineralogical com-  
717 position, *Atmos. Chem. Phys.*, 14, 10663–10686, doi:10.5194/acp-14-10663-2014, 2014a.
- 718 Formenti, P., Caquineau, S., Chevaillier, S., Klaver, A., Desboeufs, K., Rajot, J. L., Belin, S. and Briois,  
719 V.: Dominance of goethite over hematite in iron oxides of mineral dust from western Africa:  
720 quantitative partitioning by X-ray Absorption Spectroscopy, *J. Geophys. Res.*, 2014b.
- 721 Hammer, M. S., Martin, R. V., van Donkelaar, A., Buchard, V., Torres, O., Ridley, D. A., and Spurr, R.  
722 J. D.: Interpreting the ultraviolet aerosol index observed with the OMI satellite instrument to  
723 understand absorption by organic aerosols: implications for atmospheric oxidation and direct ra-  
724 diative effects, *Atmos. Chem. Phys.*, 16, 2507-2523, doi:10.5194/acp-16-2507-2016, 2016.
- 725 Hänel, G., Radiation budget of the boundary layer: Part II. Simultaneous measurement of mean solar  
726 volume absorption and extinction coefficients of particles, *Beitr. Phys. Atmos.* 60, 241-247,  
727 1987.
- 728 Hänel, G., Optical properties of atmospheric particles: complete parameter sets obtained through polar  
729 photometry and an improved inversion technique, *Appl. Opt.* 33, 7187-7199, 1994.
- 730 Harrison, R.M., Beddows, D.C.S., Jones, A.M., Calvo, A., Alves, C., and Pio, C., An evaluation of some  
731 issues regarding the use of aethalometers to measure woodsmoke concentrations, *Atmos. Envi-*  
732 *ron.* 80, 540e548, 2013.
- 733 Haywood, J. M., P. N. Francis, M. D. Glew, and J. P. Taylor, Optical properties and direct radiative  
734 effect of Saharan dust: A case study of two Saharan outbreaks using data from the U. K. Met.  
735 Office C-130, *J. Geophys. Res.*, 106, 18,417–18,430, 2001.
- 736 Haywood, J., Francis, P., Osborne, S., Glew, M., Loeb, N., Highwood, E., Tanré, D., Myhre, G., For-  
737 menti, P., and Hirst, E., Radiative properties and direct radiative effect of Saharan dust measured

- 738 by the C-130 aircraft during Saharan Dust Experiment (SHADE). 1: Solar spectrum, *J. Geophys.*  
739 *Res.*, 108(D18), 8577, doi:10.1029/2002JD002687, 2003.
- 740 Hsu, N. C., S.-C. Tsay, M. D. King, and J. R. Herman, *Aerosol Properties Over Bright-Reflecting Source*  
741 *Regions*, *IEEE Transactions Geos. Remote Sens.*, 42, 557-569, 2004.
- 742 IPCC 2013, *Climate Change 2013: The Scientific Basis, Summary for Policymakers, Working Group I*  
743 *Contribution to the Fifth Assessment Report of the Intergovernmental Panel on Climate Change*,  
744 edited by: Stocker, T. F., Qin, D., Plattner, G.-K., Tignor, M. M. B., Allen, S. K., Boschung, J.,  
745 Nauels, A., Xia, Y., Bex, V., Midgley, P. M., Cambridge University Press, Cambridge, UK, 2013.
- 746 Journet, E., Balkanski, Y., and Harrison, S. P., A new data set of soil mineralogy for dust-cycle model-  
747 ing, *Atmos. Chem. Phys.*, 14, 3801-3816, doi:10.5194/acp-14-3801-2014, 2014.
- 748 Kandler, K., Benker, N., Bundke, U., Cuevas, E., Ebert, M., Knippertz, P., Rodriguez, S., Schütz, L.,  
749 and Weinbruch, S.: Chemical composition and complex refractive index of Saharan Mineral Dust  
750 at Izaña, Tenerife (Spain) derived by elec-tron microscopy, *Atmos. Environ.*, 41, 8058-8074,  
751 10.1016/j.atmosenv.2007.06.047, 2007.
- 752 Kandler, K., Schütz, L., Deutscher, C., Hofmann, H., Jäckel, S., Knippertz, P., Lieke, K., Massling, A.,  
753 Schladitz, A., Wein-zierl, B., Zorn, S., Ebert, M., Jaenicke, R., Petzold, A., and Weinbruch, S.,  
754 Size distribution, mass concentration, chemical and mineralogical composition, and derived op-  
755 tical parameters of the boundary layer aerosol at Tinfou, Morocco, during SAMUM 2006, *Tellus*,  
756 61B, 32-50, 10.1111/j.1600-0889.2008.00385.x, 2009.
- 757 Kandler, K., Lieke, K., Benker, N., Emmel, C., Küpper, M., Müller-Ebert, D., Ebert, M., Scheuvs, D.,  
758 Schladitz, A., Schütz, L., and Weinbruch, S.: Electron microscopy of particles collected at Praia,  
759 Cape Verde, during the Saharan Mineral dust experiment: particle chemistry, shape, mixing state  
760 and complex refractive index, *Tellus*, 63B, 475-496, 10.1111/j.1600-0889.2011.00550.x, 2011.
- 761 Karickhoff, S. W. and Bailey, G. W., *Optical absorption spectra of clay minerals*, *Clays Clay Min.*, 21,  
762 59-70, 1973.
- 763 Kirchstetter, T.W., Novakok, T., Hobbs, P.V., Evidence that the spectral dependence of light absorption  
764 by aerosols is affected by organic carbon, *J. Geophys. Res.* 109, D21208, 2004.
- 765 Klaver, A., Formenti, P., Caquineau, S., Chevaillier, S., Ausset, P., Calzolari, G., Osborne, S., Johnson,  
766 B., Harrison, M., and Dubovik, O., Physico-chemical and optical properties of Sahelian and  
767 Saharan mineral dust: in situ measurements during the GERBILS campaign, *Q. J. R. Meteorol.*  
768 *Soc.*, DOI:10.1002/qj.889, 2011.
- 769 Knippertz, P., and J.-B. W. Stuut (eds.), *Mineral Dust: A Key Player in the Earth System*, DOI  
770 10.1007/978-94-017-8978-3\_\_1, Springer ScienceCBusiness Media Dordrecht, 2014.
- 771 ~~Lack, D. A., and Langridge, J. M., On the attribution of black and brown carbon light absorption using~~  
772 ~~the Angström exponent, *Atmos. Chem. Phys.* 13, 10535-10543, 2013.~~
- 773 Lafon, S., J. Rajot, S. Alfaro, and A. Gaudichet, Quantification of iron oxides in desert aerosol, *Atmos.*  
774 *Environ.*, 38, 1211-1218, 2004.
- 775 Lafon, S., Sokolik, I.N., Rajot, J.L., Caquineau, S., Gaudichet, A., Characterization of iron oxides in  
776 mineral dust aerosols: Implications for light absorption, *J. Geophys. Res.* 111, D21207,  
777 DOI:10.1029/2005JD007016, 2006.

- 778 Laskin, J., Laskin, A., Nizkorodov, S. A., Roach, P., Eckert, P., Gilles, M. K., Wang, B., Lee, H. J., and  
779 Hu, Q., Molecular Selectivity of Brown Carbon Chromophores, *Environ. Sci. Technol.*, 48,  
780 12047–12055, 2014.
- 781 Lau, K. M., K. M. Kim, Y. C. Sud, and G. K. Walker, A GCM study of the response of the atmospheric  
782 water cycle of West Africa and the Atlantic to Saharan dust radiative forcing, *Ann. Geophys.*,  
783 27, 4023–4037, doi:10.5194/angeo-27-4023-2009, 2009.
- 784 Lazaro, F. J., L. Gutiérrez, V. Barrón, and M. D. Gelado, The speciation of iron in desert dust collected  
785 in Gran Canaria (Canary Islands): Combined chemical, magnetic and optical analysis, *Atmos.*  
786 *Environ.*, 42(40), 8987-8996, 2008.
- 787 ~~Lewis, K., Arnott, W. P., Moosmüller, H., Wold, C. E., Strong spectral variation of biomass smoke light~~  
788 ~~absorption and single scattering albedo observed with a novel dual wavelength photoacoustic~~  
789 ~~instrument, *J. Geophys. Res.* 113, D16203, 2008.~~
- 790 ~~Liao, H., and Seinfeld, J.H., Radiative forcing by mineral dust aerosols: Sensitivity to key variables, *J.*~~  
791 ~~*Geophys. Res.*, 103, 31,637-31,645, 1998.~~
- 792 Lide, D. R., *CRC Handbook of Chemistry and Physics 1991 – 1992*, CRC Press, Boca Raton, Fla., 1992.
- 793 Linke, C., Möhler, O., Veres, A., Mohácsi, A., Bozóki, Z., Szabó, G., and Schnaiter, M., Optical prop-  
794 erties and mineralogical composition of different Saharan mineral dust samples: a laboratory  
795 study, *Atmos. Chem. Phys.*, 6, 3315–3323, 2006.
- 796 Loeb, N. G., and W. Su, Direct Aerosol Radiative Forcing Uncertainty Based on a Radiative Perturbation  
797 Analysis, *J. Climate*, 23, 5288, 2010.
- 798 Massabó, D., Bernardoni, V., Bove, M.C., Brunengo, A., Cuccia, E., Piazzalunga, A., Prati, P., Valli,  
799 G., Vecchi, R., A multi-wavelength optical set-up for the characterization of carbonaceous par-  
800 ticulate matter, *J. Aerosol Sci.* 60, 34-46, 2013.
- 801 Massabó, D., Caponi, L., Bernardoni, V., Bove, M.C., Brotto, P., Calzolari, G., Cassola, F., Chiari, M.,  
802 Fedi, M.E., Fermo, P., Giannoni, M., Lucarelli, F., Nava, S., Piazzalunga, A., Valli, G., Vecchi,  
803 R., Prati, P., Multi-wavelength optical determination of black and brown carbon in atmospheric  
804 aerosols, *Atmos. Environ.*, 108, 1-12, 2015.
- 805 Massabò, D., Caponi, L., Bove, M.C., Prati, P., Brown carbon and thermal-optical analysis: A correction  
806 based on optical multi-wavelength apportionment of atmospheric aerosols, *Atmos. Environ.*,  
807 125, 119-125. doi: 10.1016/j.atmosenv.2015.11.011, 2016.
- 808 ~~McConnell, C.L., E. J. Highwood, H. Coe, P. Formenti, B. Anderson, S. Osborne, S. Nava, and G. Chen,~~  
809 ~~Seasonal variations of the physical and optical characteristics of Saharan dust: results from the~~  
810 ~~Dust Outflow and Deposition to the Ocean (DODO) Experiment, *J. Geophys. Res.*, 113,~~  
811 ~~<http://dx.doi.org/10.1029/2007JD009606>, 2008.~~
- 812 ~~McConnell, C. L., P. Formenti, E. J. Highwood, and M. A. J. Harrison, Using aircraft measurements to~~  
813 ~~determine the refractive index of Saharan dust during the DODO Experiments, *Atmos. Chem.*~~  
814 ~~*Phys.*, 10(6), 3081-3098, 2010.~~
- 815 Miller, R.L., Tegen, I. and Perlwitz, J.P., Surface radiative forcing by soil dust aerosols and the hydro-  
816 logic cycle, *J. Geophys. Res.*, 109, D04203, doi:10.1029/2003JD004085, 2004.

- 817 Miller, R.L., Knippertz, P., Garcia-Pardo, C.P., Perlwitz, J.P., and Tegen, I., Impact of dust radiative  
818 forcing upon climate, *Mineral Dust*, 327-357, Springer Netherlands, 2014.
- 819 Ming, Y, Ramaswamy V, and G. Persad, Two opposing effects of absorbing aerosols on global mean  
820 precipitation, *Geophys. Res. Lett.* 37, L13701. doi:10.1029/2010GL042895, 2010.
- 821 Moosmüller, H., Chakrabarty, R. K., and W. P. Arnott, Aerosol light absorption and its measurement:  
822 A review, *J. Quant. Spectr. Rad. Trans.*, 110, 844–878, 2009.
- 823 Moosmüller, H., Engelbrecht, J. P., Skiba, M., Frey, G., Chakrabarty, R.K., and Arnott, W.P., Single  
824 scattering albedo of fine mineral dust aerosols controlled by iron concentration, *J. Geophys. Res.*,  
825 117, D11210, doi:10.1029/2011JD016909, 2012.
- 826 Moskowicz, B. M., R. L. Reynolds, H. L. Goldstein, T. S. Berquó, R. F. Kokaly, and C. S. Bristow, Iron  
827 oxide minerals in dust-source sediments from the Bodélé Depression, Chad: Implications for  
828 radiative properties and Fe bioavailability of dust plumes from the Sahara, *Aeolian Research*, 22,  
829 93-106, 2016.
- 830 Müller, T., Schladitz, A., Massling, A., Kaaden, N., Kandler, K., and Wiedensohler, A., Spectral absorp-  
831 tion coefficients and imaginary parts of refractive indices of Saharan dust during SAMUM-1,  
832 *Tellus B*, 61, 79–95, doi:10.3402/tellusb.v61i1.16816, 2009.
- 833 Patterson, E. M., D. A. Gillette, and B. H. Stockton, Complex index of refraction between 300 and 700  
834 nm for Saharan aerosol, *J. Geophys. Res.*, 82, 3153– 3160, 1977.
- 835 Pérez C., S. Nickovic, G. Pejanovic, J. M. Baldasano, and E. Özsoy, Interactive dust-radiation modeling:  
836 a step to improve weather forecasts, *J. Geophys. Res.*, 111:D16206.  
837 doi:10.1029/2005JD0067172006, 2006.
- 838 Perlwitz J., R. Miller, Cloud cover increase with increasing aerosol absorptivity—a counterexample to  
839 the conventional semi-direct aerosol effect, *J. Geophys. Res.*, 115:D08203.  
840 doi:10.1029/2009JD012637, 2010.
- 841 Perlwitz, J. P., Pérez García-Pando, C., and R. L. Miller, Predicting the mineral composition of dust  
842 aerosols – Part 1: Representing key processes, *Atmos. Chem. Phys.*, 15, 11593-11627,  
843 doi:10.5194/acp-15-11593-2015, 2015a.
- 844 Perlwitz, J. P., Pérez García-Pando, C., and R. L. Miller, Predicting the mineral composition of dust  
845 aerosols – Part 2: Model evaluation and identification of key processes with observations, *Atmos.*  
846 *Chem. Phys.*, 15, 11629-11652, doi:10.5194/acp-15-11629-2015, 2015b.
- 847 Petzold, A., Schönlinner, M., Multi-angle absorption photometry - a new method for the measurement  
848 of aerosol light absorption and atmospheric black carbon, *J. Aerosol Sci.* 35, 421-441, 2004.
- 849 Petzold, A., Rasp, K., Weinzierl, B., Esselborn, M., Hamburger, T., Dornbrack, A., Kandler, K., Schütz,  
850 L., Knippertz, P., Fiebig, M., Virkkula, A., Saharan dust absorption and refractive index from  
851 aircraft-based observations during SAMUM 2006, *Tellus B* 61: 118–130, 2009.
- 852 [Petzold, A., Veira, A., Mund, S., Esselborn, M., Kiemle, C., Weinzierl, B., Hamburger, T., Ehret, G.,](#)  
853 [Lieke, K., and Kandler, K.: Mixing of mineral dust with urban pollution aerosol over Dakar](#)  
854 [\(Senegal\): impact on dust physico-chemical and radiative properties, \*Tellus\*, 63B, 619-634, doi:](#)  
855 [10.1111/j.1600-0889.2011.00547.x, 2011.](#)



- 856 [Petzold, A., Onasch, T., Keabian, P. and Freedman, A., Interecomparison of a Cavity Attenuated Phase](#)  
857 [Shift-based extinction monitor \(CAPS PMex\) with an integrating nephelometer and a filter-based](#)  
858 [absorption monitor, Atmos. Meas. Tech., 6, 1141–1151, doi:10.5194/amt-6-1141-2013, 2013.](#)
- 859 Ravel, B., and M. Newville, ATHENA, ARTEMIS, HEPHAESTUS: data analysis for X-ray absorption  
860 spectroscopy using IFEFFIT, J. Synchrotron Radiation 12, 537–541,  
861 doi:10.1107/S0909049505012719, 2005.
- 862 Ryder, C. L., Highwood, E. J., Rosenberg, P. D., Trembath, J., Brooke, J. K., Bart, M., Dean, A., Crosier,  
863 J., Dorsey, J., Brindley, H., Banks, J., Marsham, J. H., McQuaid, J. B., Sodemann, H., and Wash-  
864 ington, R., , Optical properties of Saharan dust aerosol and contribution from the coarse mode as  
865 measured during the Fennec 2011 aircraft campaign, Atmos. Chem. Phys., 13, 303-325,  
866 doi:10.5194/acp-13-303-2013, 2013a.
- 867 Ryder, C. L., E. J. Highwood, T. M. Lai, H. Sodemann, and J. H. Marsham, Impact of atmospheric  
868 transport on the evolution of microphysical and optical properties of Saharan dust, Geophys. Res.  
869 Lett., 40, 2433–2438, doi:10.1002/grl.50482, 2013b.
- 870 Scanza, R. A., Mahowald, N., Ghan, S., Zender, C. S., Kok, J. F., Liu, X., Zhang, Y., and Albani, S.:  
871 Modeling dust as component minerals in the Community Atmosphere Model: development of  
872 framework and impact on radiative forcing, Atmos. Chem. Phys., 15, 537–561, doi:10.5194/acp-  
873 15-537-2015, 2015.
- 874 [Sertsu, S. M., and Sánchez, P. A., Effects of Heating on Some Changes in Soil Properties in Relation to](#)  
875 [an Ethiopian Land Management Practice, Soil Sci. Soc. Am. J., 42, 940–944, 1978.](#)
- 876 Shen, Z. X., J. J. Cao, R. Arimoto, R. J. Zhang, D. M. Jie, S. X. Liu, and C. S. Zhu, Chemical composition  
877 and source characterization of spring aerosol over Horqin sand land in northeastern China, J.  
878 Geophys. Res., 112, D14315, doi:10.1029/2006JD007991, 2007.
- 879 Sinyuk, A., O. Torres, and O. Dubovik, Combined use of satellite and surface observations to infer the  
880 imaginary part of refractive index of Saharan dust, Geophys. Res. Lett., 30(2), 1081,  
881 doi:10.1029/2002GL016189, 2003.
- 882 Slingo, A., et al., Observations of the impact of a major Saharan dust storm on the atmospheric radiation  
883 balance, Geophys. Res. Lett., 33, L24817, doi:10.1029/2006GL027869, 2006.
- 884 [Sokolik, I., and Toon, O., Incorporation of mineralogical composition into models of the radiative prop-](#)  
885 [erties of mineral aerosol from UV to IR wavelengths, J. Geophys. Res., 104\(D8\), 9423–9444,](#)  
886 [1999.](#)
- 887 Solmon, F., Mallet, M., Elguindi, N., Giorgi, F., Zakey, A. and Konaré, A., Dust aerosol impact on  
888 regional precipitation over western Africa, mechanisms and sensitivity to absorption properties,  
889 Geophys. Res. Lett., 35, L24705, doi:10.1029/2008GL035900, 2008.
- 890 [Sun J., Zhang, M., and Liu, T., Spatial and temporal characteristics of dust storms in China and its](#)  
891 [surrounding regions, 1960–1999: Relations to source area and climate, J. Geophys. Res.,](#)  
892 [106\(D10\), 10325–10333, 2001.](#)
- 893 [Sun, Y., G. Zhuang, Y. Wang, X. Zhao, J. Li, Z. Wang, and Z. An \(2005\), Chemical composition of dust](#)  
894 [storms in Beijing and implications for the mixing of mineral aerosol with pollution aerosol on the](#)  
895 [pathway, J. Geophys. Res., 110, D24209, doi:10.1029/2005JD006054.](#)

896 Tegen, I., and Lacis, A. A., Modeling of particle size distribution and its influence on the radiative prop-  
897 erties of mineral dust aerosol, *J. Geophys. Res.*, doi:10.1029/95JD03610, 1996.

898 Torres, O., A. Tanskanen, B. Veihelmann, C. Ahn, R. Braak, P. K. Bhartia, P. Veefkind, and P. Levelt,  
899 Aerosols and surface UV products from Ozone Monitoring Instrument observations: An over-  
900 view, *J. Geophys. Res.*, 112, *D24S47*, doi:10.1029/2007JD008809, 2007.

901 ~~Utry, N., Ajtai, T., Filep, Á., Pintér, M., Hoffer, A., Bozóki, Z., and Szabó, G., Mass specific optical~~  
902 ~~absorption coefficient of HULIS aerosol measured by a four-wavelength photoacoustic spec-~~  
903 ~~trometer at NIR, VIS and UV wavelengths, *Atmos. Environ.* 69, 321–324, 2013.~~

904 Utry, N., Ajtai, T., Filep, Á., Pintér, M., Tombacz, E., Bozóki, Z., and Szabó, G., Correlations between  
905 absorption Ångström exponent (AAE) of wintertime ambient urban aerosol and its physical and  
906 chemical properties, *Atmos. Environ.* 91, 52–59, 2014.

907 Xian, P., Seasonal migration of the ITCZ and implications for aerosol radiative impact. PhD thesis,  
908 Columbia University, 2008.

909 Vinoj, V., Rasch, P. J., Wang, H., Yoon, J.-H., Ma, P.-L., Landu, K., and Singh, B., Short-term modu-  
910 lation of Indian summer monsoon rainfall by West Asian dust, *Nat. Geosci.*, 7, 308–313,  
911 doi:10.1038/ngeo2107, 2014.

912 Wang, J., J. F. Doussin, S. Perrier, E. Perraudin, Y. Katrib, E. Pangui, and B. Picquet-Varrault, Design  
913 of a new multi-phase experimental simulation chamber for atmospheric photosimulation, aerosol  
914 and cloud chemistry research, *Atmos. Meas. Tech.*, 4, 2465–2494, 2011.

915 Wang, L., Z. Li, Q. Tian, Y. Ma, F. Zhang, Y. Zhang, D. Li, K. Li, and L. Li, Estimate of aerosol  
916 absorbing components of black carbon, brown carbon, and dust from ground-based remote sens-  
917 ing data of sun-sky radiometers, *J. Geophys. Res. Atmos.*, 118, 6534–6543,  
918 doi:10.1002/jgrd.50356, [20132016](https://doi.org/10.1002/jgrd.50356).

919 Weinzierl, B., et al., , Microphysical and optical properties of dust and tropical biomass burning aerosol  
920 layers in the Cape Verde region—an overview of the airborne in situ and lidar measurements  
921 during SAMUM-2, *Tellus B*, 63(4), 589–618, 2011.

922 Yang, M., Howell, S.G., Zhuang, J., Huebert, B.J., Attribution of aerosol light absorption to black car-  
923 bon, brown carbon, and dust in China - interpretations of atmospheric measurements during  
924 EAST-AIRE, *Atmos. Chem. Phys.* 9, 2035e2050, 2009.

925 Zhang, X. Y., Y. Q. Wang, X. C. Zhang, W. Guo, T. Niu, S. L. Gong, Y. Yin, P. Zhao, J. L. Jin, and M.  
926 Yu, Aerosol monitoring at multiple locations in China: contributions of EC and dust to aerosol  
927 light absorption, *Tellus B*, 60(4), 647–656, 2008.

928 Zhao, C., Liu, X., Ruby Leung, L., and Hagos, S.: Radiative impact of mineral dust on monsoon precip-  
929 itation variability over West Africa, *Atmos. Chem. Phys.*, 11, 1879–1893, 10.5194/acp-11-1879-  
930 2011, 2011.

931



932 **Table captions**

933 **Table 1.** Characteristics of the standards used for the quantification of the iron oxides in the XAS anal-  
934 ysis.

935 **Table 2.** ~~Summary-Geographical of~~ information on the soil samples used in this work.

936 **Table 3.** Chemical characterisation of the dust aerosols in PM<sub>10.6</sub> and PM<sub>2.5</sub> (in parentheses) size frac-  
937 tions. Columns 3 and 4 ~~report-give~~ the Si/Al and Fe/Ca elemental ratios obtained from X-Ray Fluores-  
938 cence analysis. The uncertainty of ~~fa~~ each individual value is estimated to be 10%. Column 5 ~~reports~~  
939 ~~shows~~  $MR_{Fe\%}$ , the fractional mass of elemental iron with respect to the total dust mass concentration  
940 (uncertainty 10%). Column 5 reports  $MR_{Fe\%}$ , the mass fraction of iron oxides with respect to the total  
941 dust mass concentration (uncertainty 15%). For PM<sub>2.5</sub> the determination of the Si/Al ratio is impossible  
942 due to the composition of the filter ~~medium-membranes~~ (quartz).

943 **Table 4.** Mass absorption efficiency (MAE,  $10^{-3} \text{ m}^2 \text{ g}^{-1}$ ) and Ångström Absorption Exponent (AAE) in  
944 the PM<sub>10.6</sub> and PM<sub>2.5</sub> size fractions. Absolute errors are in brackets.

945 **Table 5.** Mass absorption efficiency (MAE,  $10^{-3} \text{ m}^2 \text{ g}^{-1}$ ) and Ångström Absorption Exponent (AAE) ~~of~~  
946 ~~from the~~ literature data discussed in the paper

947

948 **Figure captions**

949 **Figure 1.** Time series of aerosol mass concentration in the chamber for ~~the~~ two companion experiments  
950 (Libyan ~~dust-sample~~). Experiment 1 (top panel) was dedicated to the determination of the chemical  
951 composition (including iron oxides) by sampling on polycarbonate filters. Experiment 2 (bottom panel)  
952 was dedicated to the determination of the absorption optical properties by sampling on quartz filters.

953 **Figure 2.** Locations (red stars) of the soil and sediment samples used to generate dust aerosols.

954 **Figure 3.** Spectral dependence of the MAE values for the samples investigated in this study in the PM<sub>10.6</sub>  
955 (left) and in the PM<sub>2.5</sub> (right) mass fractions.

956 **Figure 4.** Illustration of the links between the MAE values and the dust chemical composition found in  
957 this study. Left column, from top to bottom: linear regression between ~~the~~ MAE values ~~between-in the~~  
958 ~~range from~~ 375 ~~toand~~ 850 nm and the fraction of elemental iron ~~with-respect-to-relative to~~ the total dust  
959 mass ( $MR_{Fe\%}$ ) in the PM<sub>10.6</sub> fraction; Middle column: same as left column but ~~respect-tofor~~ the mass

960 fraction of iron oxides [relative](#) to the total dust mass ( $MR_{Fe\ ox\%}$ ) in the PM<sub>10.6</sub> size fraction; Right column:  
961 same as left column but in the PM<sub>2.5</sub> size fraction.  
962

963 **Table 1.** Characteristics of the standards used for the quantification of the iron oxides in the XAS anal-  
 964 ysis.

Standard	<del>Stoechiometric</del> Stoichiometric Formula	Origin
Illite of Puy	$(\text{Si}_{3.55}\text{Al}_{0.45})(\text{Al}_{1.27}\text{Fe}_{0.36}\text{Mg}_{0.44})\text{O}_{10}(\text{OH})_2(\text{Ca}_{0.01}\text{Na}_{0.01}\text{K}_{0.53}\text{X}(\text{I})_{0.12})$	Puy, France
Goethite	$\text{FeO} \cdot \text{OH}$	Minnesota
Hematite	$\text{Fe}_2\text{O}_3$	Niger
Montmorillonite	$(\text{Na},\text{Ca})_{0.3}(\text{Al},\text{Mg})_2\text{Si}_4\text{O}_{10}(\text{OH})_2 \cdot n(\text{H}_2\text{O})$	Wyoming
Nontronite	$\text{Na}_{0.3}\text{Fe}_2(\text{Si},\text{Al})_4\text{O}_{10}(\text{OH})_2 \cdot n\text{H}_2\text{O}$	Pennsylvania

965

966

967

968 **Table 2.** Geographical information on the soil samples used in this work.

<b>Geographical area</b>	<b>Sample</b>	<b>Desert area</b>	<b>Geographical coordinates</b>
Sahara	Morocco	East of Ksar Sahli	31.97°N, 3.28°W
	Libya	Sebha	27.01°N, 14.50°E
	Algeria	Ti-n-Tekraouit	23.95°N, 5.47°E
Sahel	Mali	Dar el Beida	17.62°N, 4.29°W
	Bodélé	Bodélé depression	17.23°N, 19.03°E
Middle East	Saudi Arabia	Nefud	27.49°N, 41.98°E
	Kuwait	Kuwaiti	29.42°N, 47.69°E
Southern Africa	Namibia	Namib	21.24°S, 14.99°E
Eastern Asia	China	Gobi	39.43°N, 105.67°E
North America	Arizona	Sonoran	33.15 °N, 112.08°W
South America	Patagonia	Patagonia	50.26°S, 71.50°W
Australia	Australia	Strzelecki	31.33°S, 140.33°E

969

970

971 **Table 3.** Chemical characterisation of the dust aerosols in PM<sub>10.6</sub> and PM<sub>2.5</sub> (in parentheses) size frac-  
 972 tions. Columns 3 and 4 give the Si/Al and Fe/Ca elemental ratios obtained from X-Ray Fluorescence  
 973 analysis. The uncertainty of each individual value is estimated to be 10%. Column 5 shows  $MR_{Fe\%}$ , the  
 974 fractional mass of elemental iron with respect to the total dust mass concentration (uncertainty 10%).  
 975 Column 5 reports  $MR_{Fe-ox\%}$ , the mass fraction of iron oxides with respect to the total dust mass concentra-  
 976 tion (uncertainty 15%). For PM<sub>2.5</sub> the determination of the Si/Al ratio is impossible due to the composi-  
 977 tion of the filter- membranes (quartz)  
 978 Chemical characterisation of the dust aerosols in PM<sub>10.6</sub> and PM<sub>2.5</sub> (in parentheses) size fractions. Col-  
 979 umns 3 and 4 report the Si/Al and Fe/Ca elemental ratios obtained from X-Ray Fluorescence analysis.  
 980 The uncertainty on each individual value is estimated to be 10%. Column 5 reports  $MR_{Fe\%}$ , the fractional  
 981 mass of elemental iron with respect to the total dust mass concentration (uncertainty 10%). Column 5  
 982 reports  $MR_{Fe-ox\%}$ , the mass fraction of iron oxides with respect to the total dust mass concentration (un-  
 983 certainty 15%). For PM<sub>2.5</sub> the determination of the Si/Al ratio is impossible due to the composition of  
 984 the filter medium.  
 985

Geographical area	Sample	Si/Al	Fe/Ca	MC <sub>Fe%</sub>	MC <sub>Fe-ox%</sub>
Sahara	Morocco	3.12 (---)	0.24 (0.28)	3.6 (4.4)	1.4 (1.8)
	Libya	2.11 (---)	1.19 (1.12)	5.2 (5.6)	3.1 (3.4)
	Algeria	2.51 (---)	3.14 (4.19)	6.6 (5.4)	2.7 (2.2)
Sahel	Mali	3.03 (---)	2.99 (3.67)	6.6 (33.6)	3.7 (18.7)
	Bodélé	5.65 (---)	12.35 (----)	4.1 (----)	0.7 (----)
Middle East	Saudi Arabia	2.95 (---)	0.29 (0.27)	3.8 (5.1)	2.6 (3.5)
	Kuwait	3.15 (---)	0.89 (1.0)	5.0 (13.6)	1.5 (4.2)
Southern Africa	Namibia	3.41 (---)	0.11 (0.10)	2.4 (6.9)	1.1 (3.1)
Eastern Asia	China	2.68 (---)	0.77 (0.71)	5.8 (13.6)	0.9 (2.5)
North America	Arizona	3.30 (---)	0.95 (----)	5.3 (----)	1.5 (----)
South America	Patagonia	4.80 (---)	4.68 (4.64)	5.1 (----)	1.5 (---)
Australia	Australia	2.65 (---)	5.46 (4.86)	7.2 (11.8)	3.6 (5.9)

986

987

988 **Table 4.** Mass absorption efficiency (MAE,  $10^{-3} \text{ m}^2 \text{ g}^{-1}$ ) and Ångström Absorption Exponent (AAE) in  
 989 the  $\text{PM}_{10.6}$  and  $\text{PM}_{2.5}$  size fractions. Absolute errors are in brackets.

		<b>PM<sub>10.6</sub></b>					
<b>Geographical area</b>	<b>Sample</b>	<b>375 nm</b>	<b>407 nm</b>	<b>532 nm</b>	<b>635 nm</b>	<b>850 nm</b>	<b>AAE</b>
Sahara	Morocco	--- (---)	--- (---)	--- (---)	--- (---)	--- (---)	--- (---)
	Libya	89 (11)	75 (9)	30 (5)	--- (---)	--- (---)	3.2 (0.3)
	Algeria	99 (10)	80 (10)	46 (7)	16 (3)	15 (3)	2.5 (0.3)
Sahel	Mali	--- (---)	103 (18)	46 (12)	--- (---)	--- (---)	--- (---)
	Bodélé	37 (4)	25 (3)	13 (2)	6 (1)	3 (1)	3.3 (0.3)
Middle East	Saudi Arabia	90 (9)	79 (8)	28 (3)	6 (1)	4 (1)	4.1 (0.4)
	Kuwait	--- (---)	--- (---)	--- (---)	--- (---)	--- (---)	2.8 (0.3)
Southern Africa	Namibia	52 (7)	49 (7)	13 (3)	5 (2)	1 (2)	4.7 (0.5)
Eastern Asia	China	65 (8)	58 (7)	32 (4)	8 (2)	7 (2)	3 (0.3)
North America	Arizona	130 (15)	99 (12)	47 (7)	21 (4)	13 (4)	3.1 (0.3)
South America	Patagonia	102 (11)	80 (9)	29 (4)	17 (2)	10 (2)	2.9 (0.3)
Australia	Australia	135 (15)	121 (13)	55 (7)	26 (4)	14 (3)	2.9 (0.3)

990  
991

PM <sub>2.5</sub>							
Geographical area	Sample	375 nm	407 nm	532 nm	635 nm	850 nm	AAE
Sahara	Morocco	107 (13)	88 (11)	34 (6)	14 (3)	15 (4)	2.6 (0.3)
	Libya	132(17)	103 (14)	33 (7)	--- (---)	--- (---)	4.1 (0.4)
	Algeria	95(8)	71 (11)	37 (7)	12 (5)	12 (5)	2.8 (0.3)
Sahel	Mali	711 (141)	621 (124)	227 (78)	--- (---)	--- (---)	3.4 (0.3)
	Bodelé	--- (---)	--- (---)	--- (---)	--- (---)	--- (---)	--- (---)
Middle East	Saudi Arabia	153 (18)	127 (15)	42 (7)	8 (4)	6 (4)	4.5 (0.5)
	Kuwait	270 (100)	324 (96)	--- (---)	54 (52)	--- (---)	3.4 (0.3)
Southern Africa	Namibia	147 (36)	131 (32)	31 (21)	6 (16)	3 (15)	5.1 (0.5)
Eastern Asia	China	201 (30)	176 (26)	89 (17)	14 (10)	23 (10)	3.2 (0.3)
North America	Arizona	--- (---)	--- (---)	--- (---)	--- (---)	--- (---)	--- (---)
South America	Patagonia	--- (---)	--- (---)	--- (---)	--- (---)	--- (---)	2.9 (0.3)
Australia	Australia	335 (39)	288 (33)	130 (19)	57 (11)	36 (9)	2.9 (0.3)

992  
993



994 **Table 5.** Mass absorption efficiency (MAE,  $10^{-3} \text{ m}^2 \text{ g}^{-1}$ ) and Ångström Absorption Exponent (AAE)  
 995 [from the efliterature](#) data discussed in the paper

Geo- graphical area	Sample	266 nm	325 nm	428 nm	532 nm	660 nm	880 nm	106 4 nm	AAE
	Morocco*								2.25– 5.13
	Morocco, PM <sub>2.5</sub> <sup>‡</sup>								2.0–6.5
Sa- hara	Morocco, submicron <sup>#</sup>	1100			60			30	4.2
	Egypt, submicron <sup>#</sup>	810			20				5.3
	Tunisia <sup>§</sup>		83			11			
	Saharan, transported <sup>μ</sup>								2.9 ± 0.2
	Saharan, transported (PM <sub>10</sub> ) <sup>°</sup>			37	27 <sup>%%</sup>	15 <sup>%%%</sup>			2.9
	Saharan, transported (PM <sub>1</sub> ) <sup>°</sup>			60	40 <sup>%%</sup>	30 <sup>%%%</sup>			2.0
Sahel	Niger <sup>§</sup>		124			19			
East- ern Asia	China <sup>§</sup>		69			10			
	China <sup>&amp;</sup>		87 <sup>&amp;</sup> &	50 <sup>&amp;&amp;&amp;</sup>	27 <sup>&amp;&amp;&amp;</sup> &	13	1		3.8
Ara- bian Penin- sula, N/NE Af- rica, Cen- tral Asia	Various locations <sup>@</sup>								2.5-3.9

996 \* Müller et al. (2008)

997 ‡ Petzold et al. (~~2008~~2009)

998 # Linke et al. (2006)

999 § Alfaro et al. (2004)

1000 <sup>μ</sup> Fialho et al. (2005)

1001 <sup>°</sup> Denjean et al. (2016); <sup>%%</sup> at 528 nm, <sup>%%%</sup> at 652 nm

1002 <sup>&</sup> Yang et al. (2009); <sup>&&</sup> at 375 nm, <sup>&&&</sup> at 470 nm, <sup>&&&&</sup> at 590 nm

1003 <sup>@</sup> Mossmüller et al. (2012)

1004

1005

1006

1007

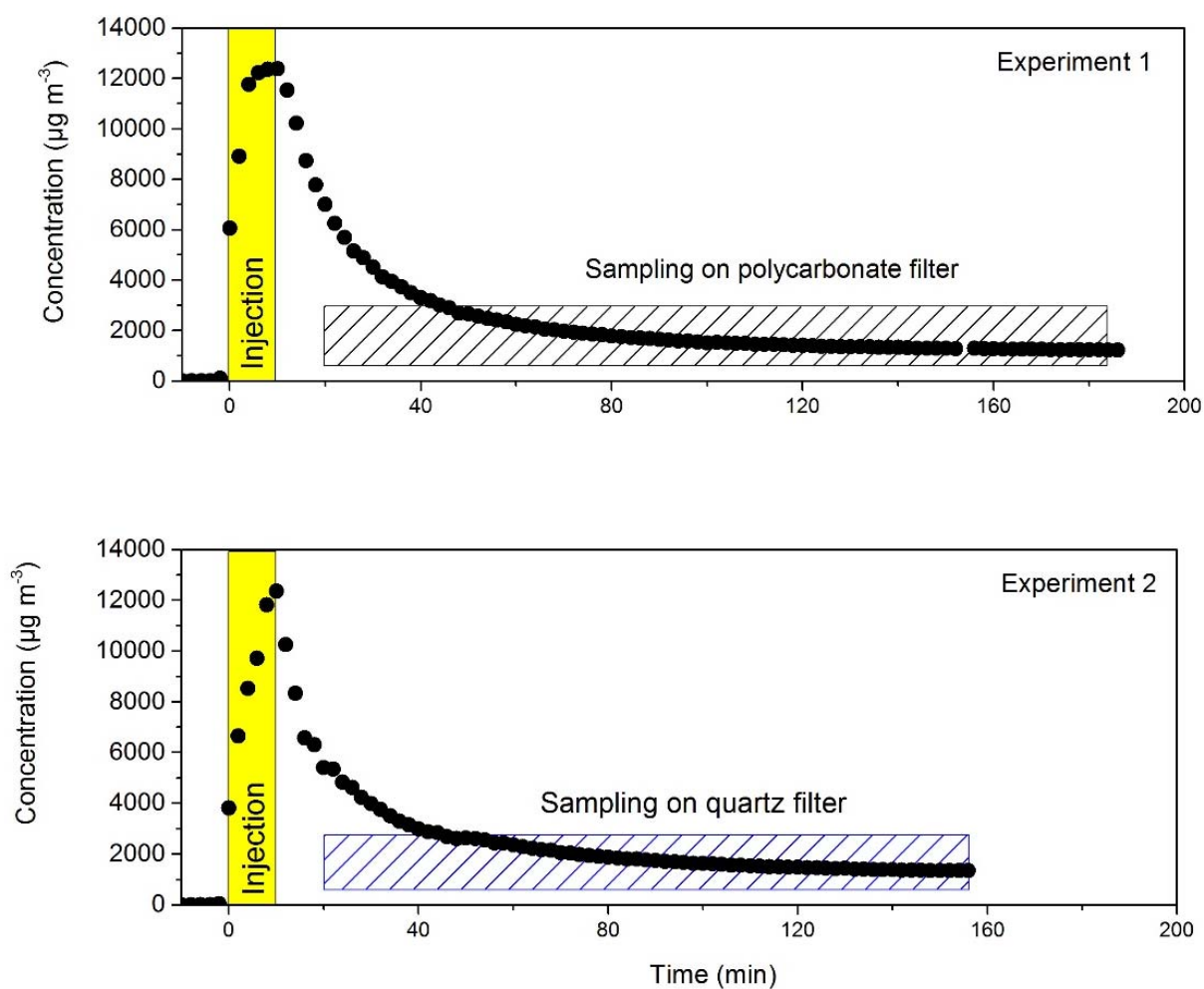
1008

1009

1010

1011

**Figure 1.** [Time series of aerosol mass concentration in the chamber for two companion experiments \(Libyan dust\).](#) ~~Time series of aerosol mass concentration in the chamber for the two companion experiments (Libya sample).~~ Experiment 1 (top panel) was dedicated to the determination of the chemical composition (including iron oxides) by sampling on polycarbonate filters. Experiment 2 (bottom panel) was dedicated to the determination of the absorption optical properties by sampling on quartz filters.

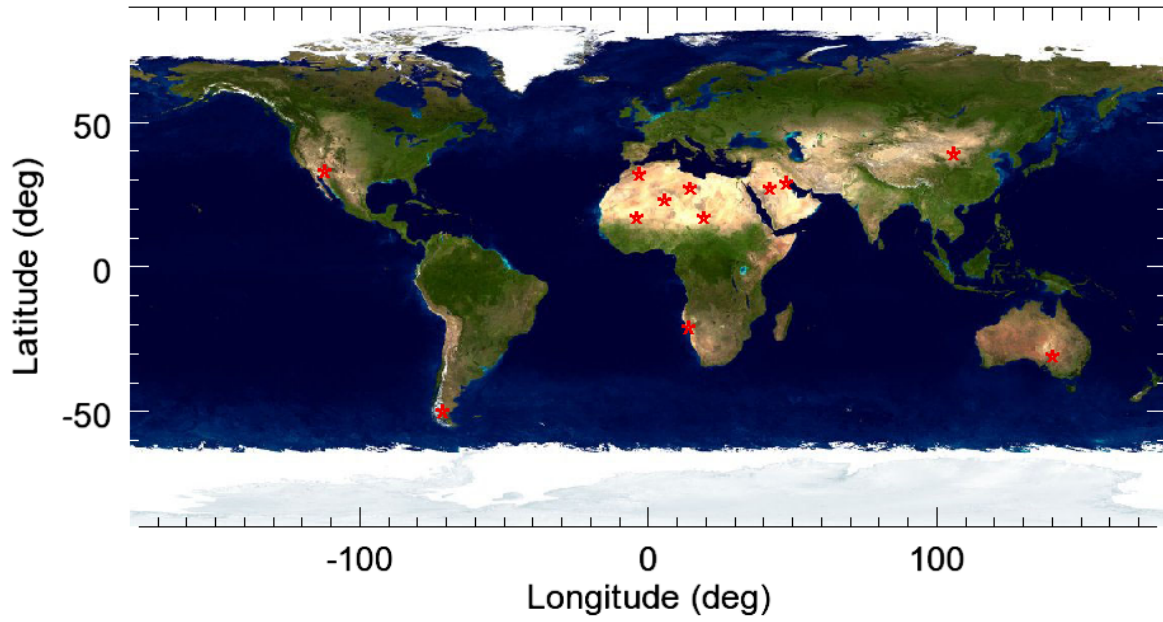


1012

1013

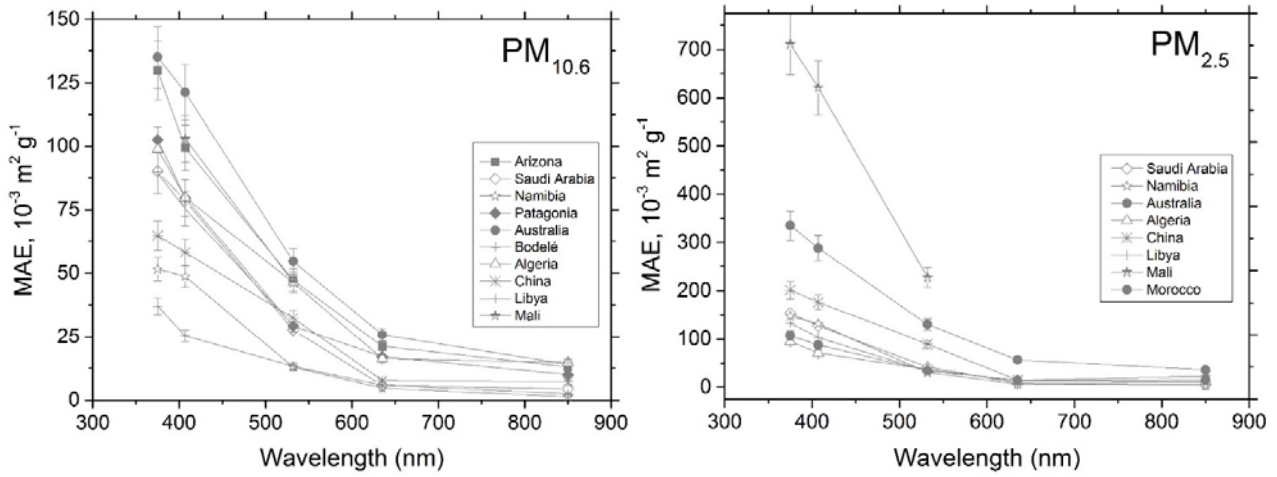
1014

1015 **Figure 2.** Locations (red stars) of the soil and sediment samples used to generate dust aerosols.



1016  
1017

1018 **Figure 3.** Spectral dependence of the MAE values for the samples investigated in this study in the PM<sub>10.6</sub>  
1019 (left) and in the PM<sub>2.5</sub> (right) mass fractions.

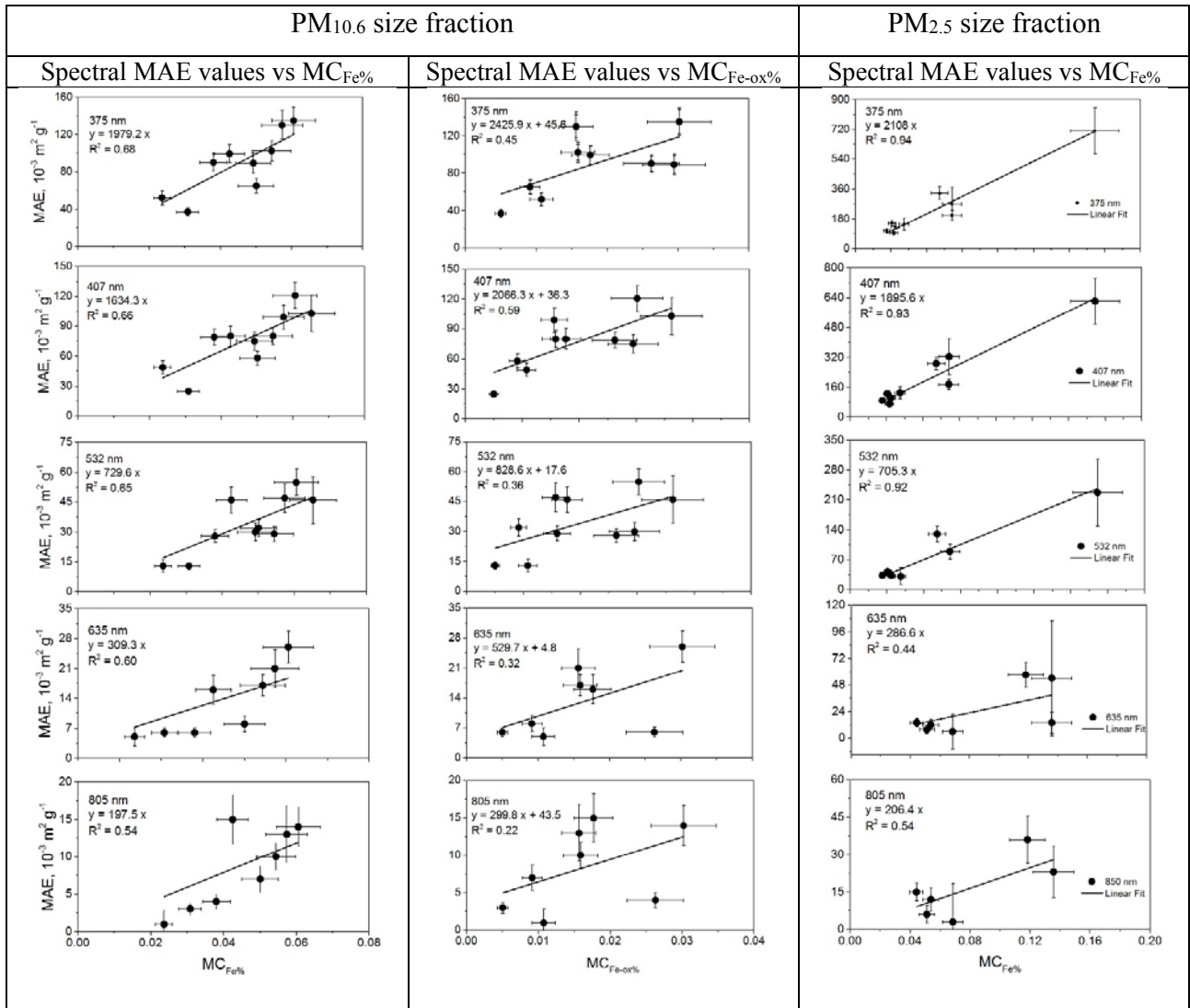


1020

1021 **Figure 4.** Illustration of the links between the MAE values and the dust chemical composition found in  
1022 this study. Left column, from top to bottom: linear regression between the MAE values in the range from  
1023 375 to 850 nm and the fraction of elemental iron relative to the total dust mass ( $MR_{Fe\%}$ ) in the  $PM_{10.6}$   
1024 fraction; Middle column: same as left column but for the mass fraction of iron oxides relative to the total  
1025 dust mass ( $MR_{Fe\ ox\%}$ ) in the  $PM_{10.6}$  size fraction; Right column: same as left column but in the  $PM_{2.5}$  size  
1026 fraction.

1027 ~~Illustration of the links between the MAE values and the dust chemical composition found in this study.~~  
1028 ~~Left column, from top to bottom: MAE values between 375 and 850 nm versus the fraction of elemental~~  
1029 ~~iron with respect to the total dust mass ( $MR_{Fe\%}$ ) in the  $PM_{10.6}$  fraction; Middle column: same as left~~  
1030 ~~column but versus the mass fraction of iron oxides to the total dust mass ( $MR_{Fe\ ox\%}$ ) in the  $PM_{10.6}$  size~~  
1031 ~~fraction; Right column: same as left column but in the  $PM_{2.5}$  size fraction. The linear regression lines~~  
1032 ~~between MAE and  $MR_{Fe\%}$  and MAE and  $MR_{Fe\ ox\%}$  are reported in each plot.~~

1033  
1034  
1035  
1036  
1037  
1038  
1039  
1040  
1041  
1042  
1043  
1044  
1045  
1046  
1047  
1048  
1049  
1050  
1051



1052  
1053